Investigation of the Accelerated Thermal Aging Behavior of Polyetherimide and Lifetime Prediction at Elevated Temperature

Chungyeon Cho, Seo Lin Nam, A. Paulina de la Mata, James J. Harynuk, Anastasia L. Elias, Hyun-Joong Chung*, Patricia I. Dolez*

C. Cho, A. Elias, H-J Chung: Department of Chemical and Materials Engineering, University of Alberta, Edmonton, Alberta T6G1H9, Canada
S. L. Nam, A. P. de la Mata, J. J. Harynuk: Department of Chemistry, University of Alberta, Edmonton, Alberta T6G 2G2, Canada
P. I. Dolez: Department of Human Ecology, University of Alberta, Edmonton, Alberta T6G 2N1, Canada

Correspondence to: Patricia I. Dolez (E-mail: pdolez@ualberta.ca) & Hyun-Joong Chung (E-mail: chung3@ualberta.ca)

Abstract

Fire-protective clothing are manufactured using heat and flame resistant fibers that are made of high-performance polymers. These polymers exhibit a gradual reduction in their performance after long-term exposure under various aging conditions. This study investigates the thermal aging behavior of a high temperature resistance polymer, polyetherimide (PEI), at elevated temperatures in air. Changes in the ultimate tensile strength (UTS), glass transition temperature, and surface properties are observed. In addition, infrared spectroscopy identifies chemical bonds in PEI being consumed because of chain scission. Applying the time-temperature superposition principle to the UTS data gives an activation energy of 112 kJ mol^{-1} for the effect of thermal aging on the mechanical strength of PEI. This value is similar to what has been reported for fire-protective clothing fabrics, which opens the possibility to use PEI as a sensing material for the development of end-of-life sensors for fire-protective fabrics.

1. Introduction

High-performance polymers are often engineered to withstand exposure to extreme conditions, such as high temperature, ultraviolet (UV) radiation, chemicals, or moisture, for use in aerospace,[1] automotive,[2] nuclear power, and other industries.[3] For example, poly etheretherketone (PEEK) has high temperature and chemical stability,[4] polysulfone (PSU) is flame retardant and has good chemical resistance properties,[5] polyphenylene sulfide (PPS) is resistant to high temperatures and chemicals,[6] polyimide (PI) has great mechanical properties, thermal stability, and chemical resistance,[7] and polyetherimide (PEI) is a thermoplastic polymer with excellent mechanical and high temperature resistance properties.[8] Due to the potential catastrophic impact of a premature failure resulting from exposure to service conditions, the estimated service life must be considered when selecting a particular polymer for a specific application.

The high performance of PEI can be associated with the functional groups in its backbone (Figure 1). These functional groups include aromatic imide groups that contribute to both mechanical stiffness and good thermal stability, and ether groups that contribute to low melt viscosity, which is a desirable property for thermal processing.[2,8] In addition, PEI has an excellent stability in hydrolytic environments such as diluted bases and mineral acids (for short-term contact).[2] Therefore, PEI has been used in applications under high temperature and moisture prone environments,[9] and is frequently found in electronics,[10] automotive (i.e., vehicle headlamps),[2] medical,[11] and aircraft[12] applications.

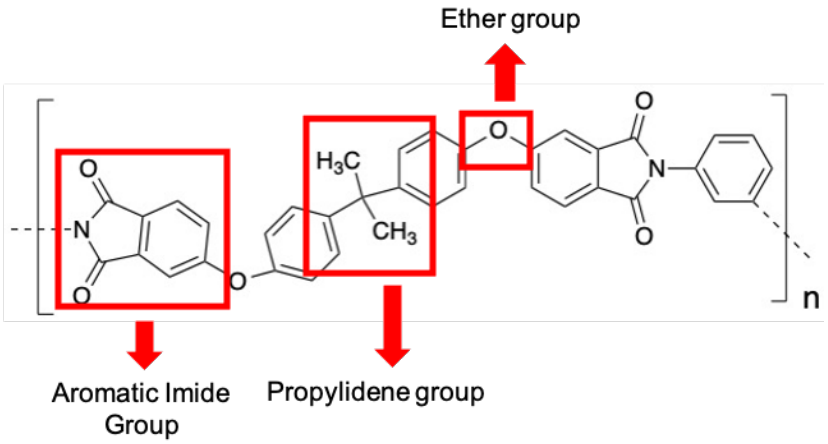

Figure 1: Chemical structure of polyetherimide and its functional groups.

However, long term exposure of polymers to severe environments may lead to a progressive reduction in performance due to aging. Chemical aging is a process involving changes at the molecular scale such as chain scission and crosslinking.[13] For instance, chain scission causes a decrease in molecular weight distribution. Chemical aging can also lead to the formation/consumption of chemical bonds. Decreases in molecular weight can cause a reduction in the tensile strength and elongation at break, while crosslinking can increase tensile strength.[14] The formation of new chemical bonds can generate visual changes, such as in color or transparency.[13]

The thermal degradation behavior of PEI has been studied and possible degradation mechanisms have been suggested.[8,15–17] Amancio-Filho et al. investigated PEI plates that were joined by friction riveting (FricRiveting), which caused their thermal degradation.[8] They observed that the chemical properties of the PEI plates changed depending on the rotating speed of the aluminum rivet. The heat generated led to a temperature increase of 350 °C to 475 °C depending on the rotating speed of the rivet (1570 to 2200 rad s^{-1}). The authors reported that these temperatures are above the onset of chain scission in PEI. This led to a 10% reduction in the molecular weight at the highest rotating speed. Fourier-transform infrared spectroscopy (FTIR) analysis showed that the absorbance of the main groups of PEI decreased with increasing the rotation speed. Carroccio et al. investigated the thermal degradation mechanism of PEI by direct pyrolysis with mass spectrometry.[15] The authors used mass spectrometry for identifying the pyrolysis products of PEI. The pyrolysis of meta-aramid was performed for comparison. It was found that meta-aramid and PEI yield the same type of pyrolysis products beyond 550 °C.

Thermogravimetry has been coupled with mass spectroscopy and FTIR to study the thermal degradation behavior of five different aromatic PEI compounds in an inert atmosphere (helium) and air.[16] This test was conducted between 25 and 620°C in air and between 25 and 680°C in helium. The thermal stability was lower in air than in helium for three of the five PEI compounds and similar for the other ones, which had an oxadiazole derivative as a substitute in the side chain. These two compounds also had the lowest thermal stability. Depending on the PEI compound, the authors suggested that the decomposition mechanisms involve the scission of 1,3,4-oxadiazole group and/or degradation of the bisphenol A unit, polyimide group, and/or triphenylmethane group.

In another study, PEI thin film specimens were subjected to thermal aging in air-ventilated ovens and autoclaves at two different oxygen partial pressures (0.21 and 50 bars) for up to 15,000

hours.[17] Thermal aging was performed at two temperatures below the glass transition (T_g) of PEI (180 and 200°C) and two temperatures above T_g (220 and 250°C). The chemical changes due to thermal aging were assessed by FTIR on specimens collected after different aging times. The authors observed a decrease in the IR absorption bands at 2970, 2935, and 2875 cm^{-1} and an increase in the absorption bands between 3700 and 3200 cm^{-1}. These changes in the absorption bands were attributed to oxidation taking place in the bisphenol A unit in the PEI molecule. They were observed at all aging times for samples aged at 220 and 250°C, but were only detected for aging times beyond 4,000 hours at aging temperatures below Tg. The effect of thermal aging at 220 and 250°C on the Young's modulus of the polymers was assessed by micro-indentation measured on the cross section of thicker PEI plates. The authors reported the formation of an oxidized layer on both surfaces of the specimens.

Finally, a recent study looked at the thermal degradation behavior and lifetime estimation of PEI/carbon fiber composite.[18] When heated from 25 to 1000 °C at different heating rates (2, 4, 6, 8, and 10 °C min^{-1}), PEI experienced a 17 to 21 % weight loss, while the carbon fibers were relatively stable. This study defined the lifetime of the PEI/carbon fiber composite as the time when the sample had undergone a 5 % weight loss, as measured by thermogravimetric analysis. The lifetime was calculated to be 1.3×10^{12} years at 80 °C, which is the highest service temperature of commercial aircrafts, the main application for PEI/carbon fiber composites. At room temperature, the lifetime was predicted to be 5.3×10^{17} years. However, this estimation was based on experiments conducted in an inert atmosphere. In addition, it did not consider realistic service situations, which could involve other conditions such as weathering and mechanical loadings.

To further the understanding of PEI thermal aging in environments simulating real use scenarios, this study investigates the thermal aging behavior of PEI films in air at different temperatures below T_g, and characterizes the resulting changes in its mechanical and chemical properties. Based on the data obtained, the activation energy of PEI was estimated using the time-temperature superposition principle. Furthermore, FTIR was used to identify possible mechanisms involved in the aging of PEI. This study gives new perspectives on the understanding of the aging mechanisms and prediction of service life of high-performance polymers under extreme conditions.

2. Experimental Section

PEI specimens (described in Section 2.1) were subjected to thermal aging at three different temperatures (190, 200 and 210 °C) and at least 10 exposure times. For each condition, eight replicate samples were produced. The residual mechanical performance and surface condition were assessed on the specimens aged at these three temperatures. In addition, FTIR analysis, differential scanning calorimetry (DSC), and thermogravimetric analysis (TGA) were performed on specimens aged at the highest temperature (210 °C). FTIR measurements were performed on the dog-bone-shaped specimens used for the tensile tests before tensile testing was carried out. Complementary surface analysis by scanning electron microscopy (SEM) and atomic force microscopy (AFM) was conducted.

2.1. Materials and specimen preparation

Eight 80 μm thick PEI films (Ultem) were purchased from McMaster Carr (Elmhurst, IL, USA). Dog-bone shape samples in accordance with ISO 527[19] were hand cut using a metal template. The specimens had a gauge length of 25 mm, a width of 4 mm, a thickness of 0.8 mm, and an overall length of 75 mm. This technique of preparation of the dog-bone specimens was selected as it yielded a lower variability in the strength results compared to the other strategies (laser and die cutting of the PEI films) investigated during initial experiments for this study (data not shown).

A total of 41 dog-bone specimens were cut from each PEI film. To minimize the effect of the inter-film variability, each film included one individual specimen for each time/temperature condition. The 41 specimens from each film were used as follows: one specimen as a control (unaged film), 30 specimens used for testing the three different aging temperatures and 10 different aging times at each temperature, and 10 extra specimens. The details of the dog-bone specimen preparation are provided in the Supporting Information.

2.2. Accelerated thermal aging program

The thermal aging of the dog-bone specimens was undertaken in air at 190, 200 and 210 °C. The temperature of 210 °C is just below the glass transition temperature of PEI (around 217 °C, see section 3.1).The lowest temperature selected for accelerated thermal aging (190 °C) corresponds to the thermal index of para-aramid fibres, which have the lowest value among

inherent flame resistant fibres.[20] The specimens were placed in a convection oven (Heratherm™, ThermoFisher Scientific, Ottawa, ON, Canada) for designated time periods (190 °C: up to 12 weeks, 200 °C: up to 16 weeks, and 210 °C: up to 8 weeks). Information about the temperature distribution in the oven is provided in the supporting information (section S1). Specimens were positioned so that the replicate samples for each condition were distributed across the oven (details in the supporting information section S2).

2.3. Mechanical characterization

A tensile testing frame (Instron 5943, Instron, Norwood, MA, USA) equipped with a 1 kN load cell was used to measure the ultimate tensile strength of the PEI dog-bone specimens. The dog-bone specimens were tested at a constant strain rate of 10 mm min^{-1} until failure according to the standard test method ISO 527.[19] For each aging time and temperature condition, the ultimate tensile strength was measured on the eight replicate samples; average values and standard deviations were determined. All tests were carried out at room temperature and atmospheric pressure.

2.4. Chemical analysis by Fourier Transform Infrared (FTIR) Spectroscopy with Attenuated Total Reflection (ATR)

FTIR spectra were recorded using a Nicolet™ Continuum™ FTIR Microscope (Thermo Scientific). The main bench is a Nicolet 8700 equipped with a narrow-band mercury cadmium telluride (MCT) detector and a micro-ATR accessory with a Ge tip (Thermo Scientific). For the measurement, specimens were placed on a support and the Ge crystal tip was lowered to contact the sample. Spectra were recorded in the range from 4000 cm^{-1} to 650 cm^{-1} at 4 cm^{-1} resolution. 128 scans were averaged for each acquisition (background and sample). For each condition, eight dog-bone specimens (one per film) were analyzed on the narrow neck of the dog-bone; two additional measurements were taken on two specimens (of the eight) as replicates. Control samples were measured (one per film with two replicates) using identical conditions as for the aged samples.

2.5. Scanning electron microscopy (SEM)

The surface details of the control and aged PEI specimens were observed by a field emission scanning electron microscope (FE-SEM, Zeiss Sigma, Germany, 5 kV). A gold coating was sputtered onto the surface of the PEI at a pressure of 100 mTorr and a current of 15 mA for 1 min (Denton Vacuum Sputter DESK II, Denton, NJ, USA). The layer of gold deposited on the PEI specimens was approximately 8 nm thick.

The crack surface area on the aged PEI samples was determined from the SEM images. Five different spots per sample (44.42 μm^2 per spot area, 222.1 μm^2 for five spots area) were used to estimate the crack surface area. The color histogram feature in ImageJ (NIH, Bethesda, MD, version 1.8.0.172) was used to perform the quantitative analysis of the crack surface area. First, the contrast and brightness were adjusted on the imported SEM images to intensify the crack area. Second, the color histogram feature in the software was used to display the cracks in black, while the rest of the surface was red. This process is illustrated in supporting information section S3. The "Analyze histogram" feature of the software then reported the number of black and red pixels in the image. Finally, the ratio of black vs. red pixels in the image was calculated, and was used to determine the crack surface area, as described by Equation 1.

$$\text{Crack surface area (\%)} = \frac{\text{Number of black pixels (crack)}}{\text{Total number of pixels in the image}} \times 100 \quad (1)$$

2.6. Differential scanning calorimetry (DSC)

The effect of thermal aging on the glass transition temperature of PEI was determined by differential scanning calorimetry (DSC, Q1000, TA Instruments, DE, USA). A small section of the dog-bone specimens exposed to thermal aging was used for the DSC testing. For the measurement, a 2 mg sample was sealed in an aluminium sample pan and exposed to the following thermal conditions: (1) hold at 25 °C for 3 min, (2) heat from 25 °C to 350 °C at a rate of 20 °C min^{-1}, (3) hold at 350 °C for 3 min, (4) cool down to 25 °C at a rate of 20 °C min^{-1}. The heat flow as a function of the temperature was recorded. The onset and end points in the resulting DSC curve were determined using the Bi-Gaussian fitting provided by the Peak Analyzer function in Origin (Version 2020b, Originlab.com). The curve fitting process is shown in Figure S7, and T_g was

determined as the mid-point between the onset and the end point, as described in supporting information section S4.

2.7. Thermogravimetric analysis (TGA)

The effect of thermal aging on the thermal decomposition of PEI was studied by thermogravimetric analysis (Discovery TGA, TA Instruments, New Castle, DE, USA). Samples with a mass of 2 mg were taken from control and aged PEI dog-bone specimens. These samples were heated from 30 °C to 850 °C in air with a flow rate of 25 mL min^{-1} and a heating rate of 20 °C min^{-1} in the thermal analyzer. The variation in the sample weight was recorded as a function of the temperature.

2.8. Atomic Force Microscope (AFM) and optical microscope analysis

The surface roughness of the PEI samples was measured using an atomic force microscope (Dimension Edge™, Bruker). The microscope was operated in the tapping mode and an area of 50 μm × 50 μm (512 × 512 points) was scanned at a scan rate of 0.6 Hz. Measurements were performed at five different points of the specimen surface and the results were averaged for each condition.

In addition, unique patterns on the PEI films were observed using an optical microscope (Stereomaster, Fisher Scientific).

2.9. Statistical Analysis

Depending on the experimental methods, measurements were generally performed 3 to 8 times and mean values were used to identify changes resulting from exposure of the PEI specimens to thermal aging. Where applicable, statistical significance was evaluated using single factor ANOVA analysis. A confidence level of 0.05 was set to establish significance. The details of post-hoc analysis are included in the supporting information sections S5 to S8.

3. Results and discussion

3.1. Thermal properties

The TGA curves of the PEI samples in the unaged condition and after thermal aging for 4, 6 and 8 weeks at 210 °C are shown in Figure 2. Two distinct stages of degradation can be seen above 500 °C. As described in the literature, the first stage corresponds to the decomposition of aliphatic chains, while the second stage corresponds to the decomposition of aromatic groups.[21] Figure 2 b) and Figure 2 c) show enlarged views of these two zones. The decomposition behavior of the PEI samples was characterized using the following parameters: $T_{5\%}$, which is defined as the decomposition temperature corresponding to a weight loss of 5%;[21] $T_{initial}$, which is the temperature of onset of the weight loss of the sample;[22] $T_{1st\ max\ rate}$, which is the temperature at which the highest rate of weight loss occurs in the first decomposition region; and $T_{2nd\ max\ rate}$, which is the temperature at which the highest rate of weight loss occurs in the second decomposition region.[21]

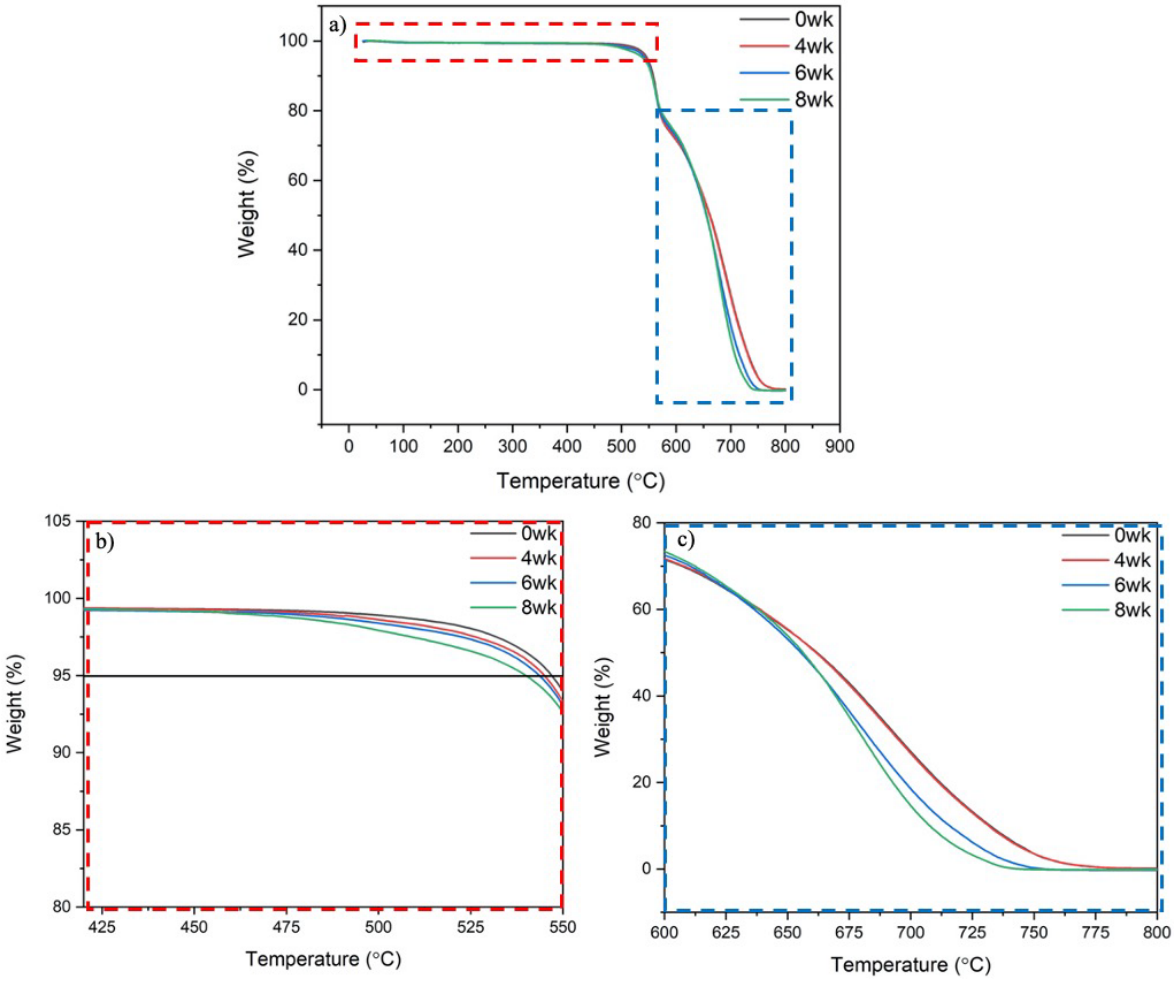

Figure 2: a) TGA curves of PEI controls and after thermal aging for 4, 6 and 8 weeks at 210 °C, b) Enlarged view of $T_{initial}$, showing the first deflection point from the baseline, corresponding to the decomposition of aliphatic groups (the black solid line indicates 5 % weight loss), c) Enlarged view of $T_{2nd\ max\ rate}$ corresponding to the decomposition of the aromatic groups in PEI.

The values of these parameters are shown in Table 1, both for the control condition and after thermal aging for 4, 6 and 8 weeks at 210 °C. The values for the control PEI specimens are in agreement with the literature.[15] An 8% decrease in the mean value of $T_{initial}$ is observed with 8 weeks of aging at 210 °C. This decrease in the mean value of $T_{initial}$ might be attributed to chain scission in PEI during thermal aging.[21] A slight decrease is observed in the mean $T_{5\%}$ value between the control condition and 8 weeks of aging. $T_{1st\ max\ rate}$ (corresponding to the aliphatic groups) did not appear to change with increased aging times. The mean $T_{2nd\ max\ rate}$ values (corresponding to the aromatic groups) decreased by 3% between the control condition and 8 weeks of aging at 210 °C. The overall statistical analysis showed that only one condition pair (control vs. 8 weeks) was statistically different from each other for the $T_{initial}$ and $T_{5\%}$ values, while the $T_{1st\ max\ rate}$ and $T_{2nd\ max\ rate}$ values were not statistically different.

Table 1: Values of the parameters extracted from the TGA curves for PEI in the controls and after thermal aging for 4, 6 and 8 weeks at 210 °C.

Parameter / **Condition**	**$T_{5\%}$ (°C)**	**$T_{initial}$ (°C)**	**$T_{1st\ max\ rate}$ (°C)**	**$T_{2nd\ max\ rate}$ (°C)**
Control	548 ± 1	480 ± 3	562 ± 1	685 ± 8
4 weeks	545 ± 2	460 ± 6	564 ± 1	690 ± 2
6 weeks	544 ± 1	466 ± 8	560 ± 3	681 ± 3
8 weeks	540 ± 1	442 ± 6	565 ± 2	663 ± 2

Figure 3 presents the effect of thermal aging on the thermal behavior of PEI as measured by DSC. The results shown in Figure 3 correspond to the following four conditions: control, and aged for 4, 6 and 8 weeks at 210 °C. This aging temperature was chosen as it is slightly lower than the

glass transition temperature of the polymer (around 217 °C, as discussed below). In each of the aged samples, an endothermic peak is visible between 220 and 230 °C, whereas the control sample did not show such a peak. In the case of the thermally aged PEI samples reported here, this DSC peak might have been caused by the crosslinking and chain scission reactions taking place during thermal aging. When a polymer is thermally aged, both crosslinking and chain scission reactions occur. Initially, thermal aging mainly involves crosslinking taking place in the polymer network; in the second stage of aging, chain scission reactions break apart the polymer network, broken bonds create radicals and these radicals can react with either each other or oxygen and form new bonds.[13] Chemical bond formation is exothermic, and is accompanied by heat and energy loss.[23] When an aged polymer is heated above its T_g during the DSC test, the polymer absorbs heat which may correspond to the amount of energy lost during thermal aging.[24] Therefore, the endothermic peak observed in the DSC curves of the aged specimens just above T_g can potentially be attributed to the energy lost through crosslinking and formation of new bonds during the aging process. The fact that the values of this endothermic peak area for samples aged at 210 °C for 4, 6, and 8 weeks are not statistically different (96.0 ± 0.9, 92 ± 3, and 88 ± 4 J g^{-1}, respectively and a p-value of 0.21) may point to crosslinking reactions that occurred during the early stage of aging as the source of this phenomenon.

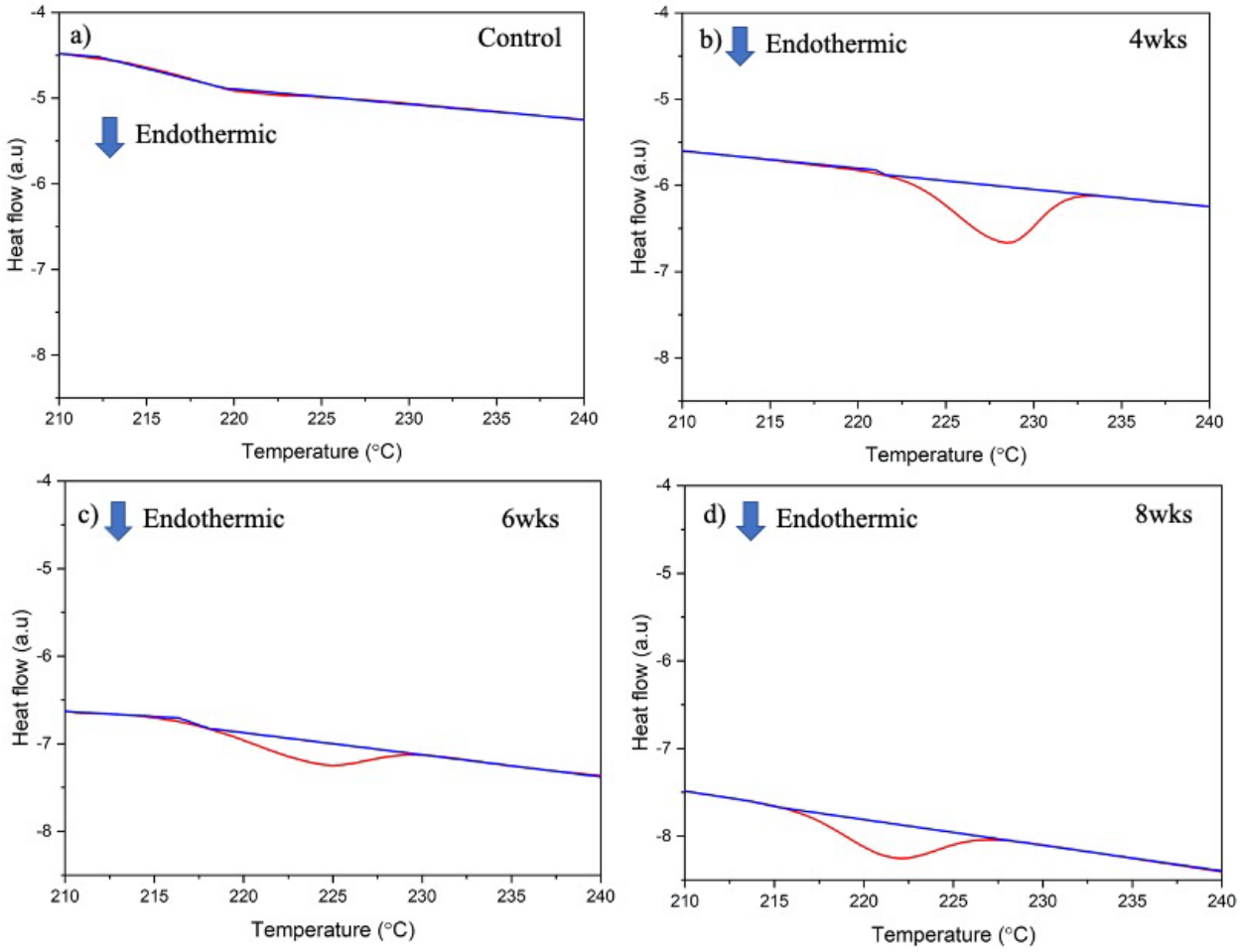

Figure 3: Differential scanning calorimetry curves (red curve) measured for PEI samples a) control and after thermal aging at 210 °C for b) 4 weeks c) 6 weeks and d) 8 weeks. The onset and end point are determined using the tangent technique (blue lines).

Table 2 gives the values of T_g corresponding to the conditions shown in Figure 2 (the T_g values were determined according to the method described in section 2.6). The value of T_g for the control PEI specimens is in agreement with the literature.[25] The mean value of T_g increased slightly between the control condition and 4 weeks of aging, and then decreased with further aging. A statistical analysis of the results was made (supporting information section S6). All conditions were found to be significantly different from the other conditions except for one pair: 0 week vs. 8 weeks. The initial increase in T_g may be attributed to a crosslinking reaction taking place at the beginning of the aging process, which restricts molecular mobility.[26–28] Further thermal aging (beyond 4 weeks) induced chain scission; thus, the value of T_g decreased for 6 weeks and 8 weeks of aging due to the increased chain mobility.

Table 2: Values of the glass transition temperature of PEI before aging and after thermal aging at 210 °C for 4, 6 and 8 weeks. The average value and standard deviation are calculated for 5 measurements.

Aging condition at 210 °C	T_g (°C)
Control	216.8±0.6
4 weeks	222.5±0.5
6 weeks	218.7±0.3
8 weeks	216.4±0.5

3.2. Mechanical properties

The effect of thermal aging on the tensile properties of the PEI specimens was characterized for different aging times and temperatures: up to 12 weeks at 190 °C, up to 16 weeks at 200 °C, and up to 8 weeks at 210 °C. The ultimate tensile strength (UTS) was determined for each specimen. The variation of the UTS averaged over the eight replicate samples as a function of the aging time and temperature is shown in Figure 4. The individual data points corresponding to each individual sample are also included. An example of stress-strain curve of an aged PEI specimen (210 °C, 8 weeks) is shown in Figure S9 in the supporting information section S9.

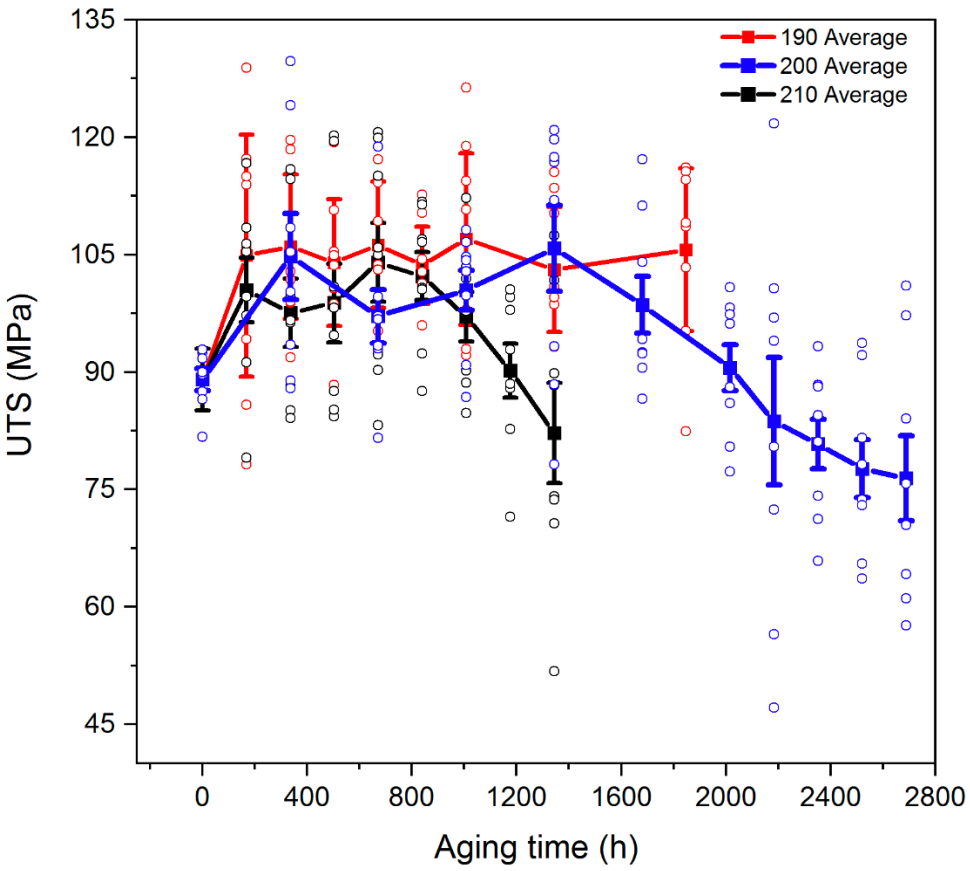

Figure 4: Variation of the specimen UTS as a function of aging time for three aging temperatures, 190, 200 and 210 °C. The open circles correspond to individual UTS values for the eight replicate samples, with their color referring to the relevant aging temperature (as shown in the legend), while the solid circles correspond to the mean values. The lines between the mean values are provided as a guide for the eye.

The average UTS of the control PEI specimens was 90 ± 4 MPa. After the first week of aging, the UTS value increased by 13-17 % for all aging temperatures. This increase in the UTS is attributed to the crosslinking reaction that may take place during the initial stages of thermal aging.[29] This is consistent with the increase in T_g observed between the control condition and 4 weeks of aging at 210°C (Table 2). In the case of thermal aging at 190 °C, the UTS increased by around 20 % during the first week (as compared with the control condition) and then remained fairly constant until the end of the aging program at 12 weeks. The increased scattering generally observed in the individual UTS values of the aged PEI specimens at 190 °C compared to the control condition can be attributed in part to the fact that aging of polymers is by definition an

inhomogeneous process. In addition, small variations have been measured in the oven temperature distribution (supporting information, section S1). Specimens located close to the oven door may have also experienced a larger temperature drop when the oven door was opened to collect specimens at regular intervals, resulting in differences in the properties of the samples.

On the other hand, when thermal aging was performed at 200 and 210 °C, the UTS of the PEI specimens increased initially, reached a plateau, and then began to decrease with increasing aging time. The decrease in the UTS value started after eight weeks of aging at 200 °C, and after 4 weeks of aging at 210 °C. These higher temperatures allowed the aging process to reach its second step, with the occurrence of chain scission.[30] This result is consistent with the decrease in the glass transition temperature observed after 4 weeks of aging at 210°C (Table 2). Other studies of thermal aging of polymeric materials have also shown similar changes in their mechanical properties as a function of aging time and temperature. For instance, Yang et al. studied the effect of thermal aging on the mechanical properties of PEEK.[31] The tensile strength of the PEEK samples increased during short aging times, but decreased for longer aging times. The study concluded that the increase of the mechanical properties was linked to crosslinking in the polymer network, while the decline in mechanical properties was due to chain scission. In the case of cross-linked polyethylene (PE), Mecheri et al. showed that the samples underwent a decrease in tensile strength of 30 % to 70 % depending on the aging time and temperature.[32] Sirisinha et al. studied the effect of thermal aging on the mechanical properties of a chlorinated PE/natural rubber blend.[33] The different ratios of the PE/rubber blend underwent a decrease in tensile strength of 36 % to 50 % due to aging, with samples with higher rubber content undergoing a larger decrease.

Following the work by Parkman, who analysed the creep and relaxation of a PEI cylinder subjected to constant radial deformation,[34] the time-temperature superposition (TTS) principle was used to construct a master curve from the UTS data for the specimens exposed to accelerated aging at 200 and 210 °C (Figure 5). The values at 200 °C were used as the reference. The data at 190 °C could not be used in this analysis as the second stage of the thermal aging process corresponding to the decrease in UTS was not reached. The shift factors provided by the TTS transformation are displayed on an Arrhenius plot (inset in Figure 5). If the UTS data can be described by an Arrhenius model, the plot of the logarithm of the shift factors as a function of the inverse of the absolute temperature will show a linear relationship as described in Equation (2).[35] In Equation (2), a_T are the shift factors, T and T_{ref} are the absolute temperatures of the shifted and

the reference data, respectively, E_a is the activation energy of the degradation process leading to the loss in performance, and R is the universal gas constant (8.31 J K^{-1} mol^{-1}). Here, since only the data at two aging temperatures are used to construct the TTS master curve, it is not possible to verify that the Arrhenius model applied for the thermal aging of PEI. However, several studies have successfully used the Arrhenius model to described the effect of thermal aging on the mechanical strength of other polymers, e.g. polychloroprene,[36] polyamide,[37] para-aramid/polybenzimidazole (PBI) blend yarns and fabrics,[38] and various fire-protective fabric blends.[39] In addition, the Arrhenius model was shown to apply to the tensile creep of PEI/carbon fibre at different temperatures.[40] Therefore, this curve was used here to compute the value of the activation energy corresponding to the effect of thermal aging on the UTS of PEI using Equation (2). The value provided by the TTS shift factors is 112 kJ mol^{-1}. This value is similar to the values of activation energy reported for fire-protective fabric blends used as outer shell in firefighter protective clothing,[39] with for instance an activation energy of 111 kJ mol^{-1} for a 60/40 Kevlar®/PBI fabric and of 113 kJ mol^{-1} for a 60/40 Kevlar®/Nomex® IIIA (93% Nomex®, 5% Kevlar®, 2% carbon fibers) fabric. Even if some uncertainty exists in the exact value of the activation energy for PEI since the Arrhenius plot only includes two data points, the similarity of the values shows that PEI offers an interesting potential as a sensing material for the development of end-of-life sensors for fire-protective fabrics.

$$a_T = exp\left[\frac{E_a}{R}\left(\frac{1}{T_{ref}} - \frac{1}{T}\right)\right] \quad (2)$$

The Hill equation has been successfully used by researchers to fit the sigmoid curves corresponding to the TTS master curve of the effect of thermal aging on the tear strength of a series of fire-protective fabric blends.[39] The 4-parameter Hill equation (Equation 3) was used to fit the data in Figure 5 corresponding to the TTS master curve of the effect of thermal aging on the UTS of PEI.

$$y = F_0 + (F_\infty - F_0)\frac{x^n}{x^n + k^n} \quad (3)$$

In Equation 3, *n* corresponds to the slope of the fitted curve, F_0 is the initial UTS value (control) and F_∞ is the value of the lower asymptote. *k* relates to the inflection point, which indicates the degradation rate (a higher *k* value retards as much as possible the degradation). Based on this fitting of the TTS master curve by the 4-parameter Hill equation, the following values were obtained for

the parameters: $n = 5.6$, $F_0 = 102$ MPa, $F_\infty = 46$ MPa, $k = 2670$ h. The values of n and k are similar to the values obtained for the thermal aging of various outer shell fabrics.[39]

The master curve (Figure 5) can also be used to estimate the lifetime of the material. If 50% of UTS retention is selected as the criterion for the termination of use (green star in Figure 5), [35] the lifetime can be estimated to be 188 days at 200 °C and 113 days at 210 °C.

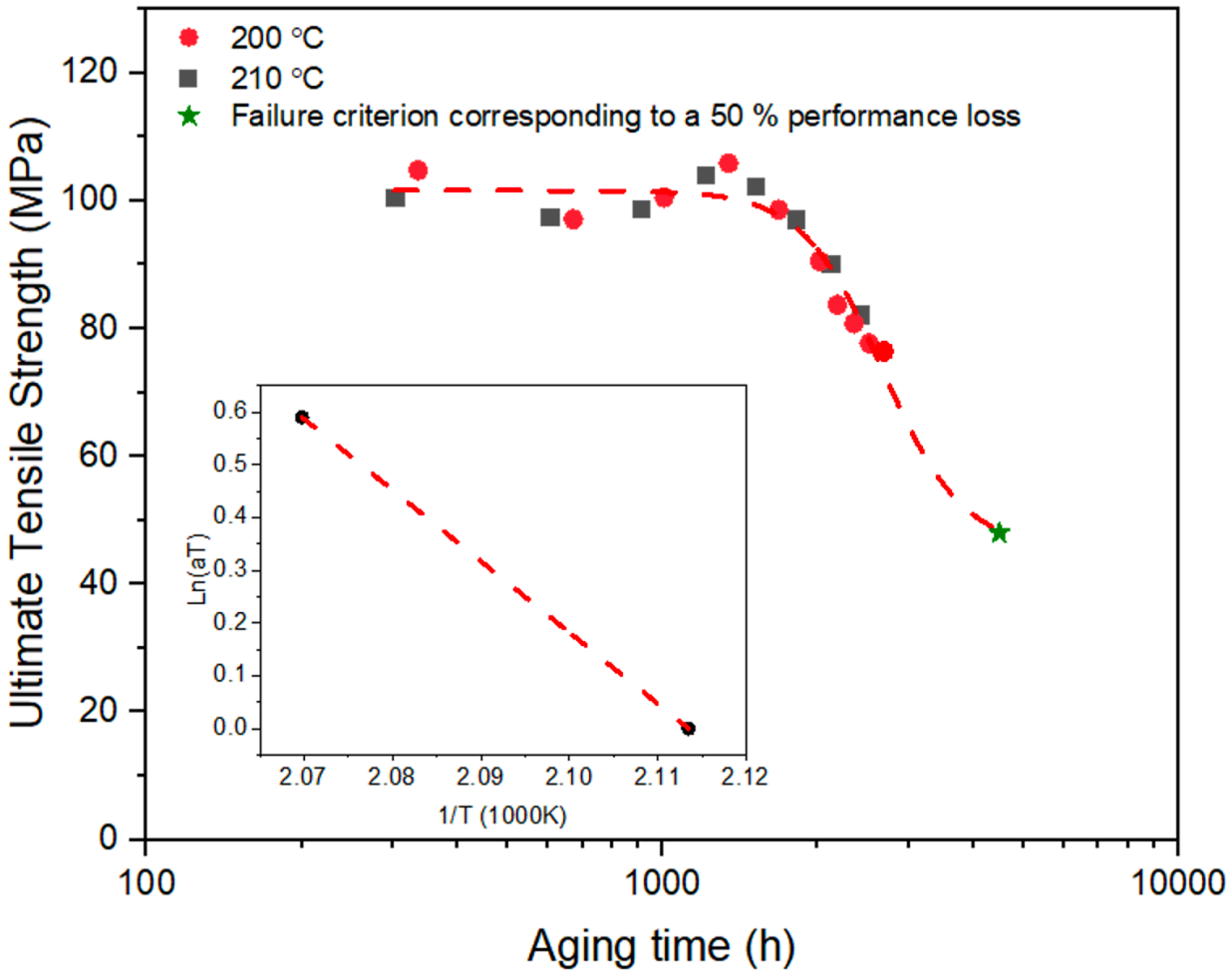

Figure 5: TTS master curve at a temperature of 200 °C for the thermal aging of PEI (insert: Arrhenius plot of the shift factors).

3.3. ATR-FTIR analysis

The chemical changes that took place in the PEI samples during thermal aging were investigated by ATR-FTIR spectroscopy. The pre-treated FTIR spectra (with the baseline correction and normalization by the reference peak area, details in the supporting information

section S10) at different thermal aging times (0, 2, 4, 6 and 8 weeks) for an aging temperature of 210 °C are shown in Figure 6.

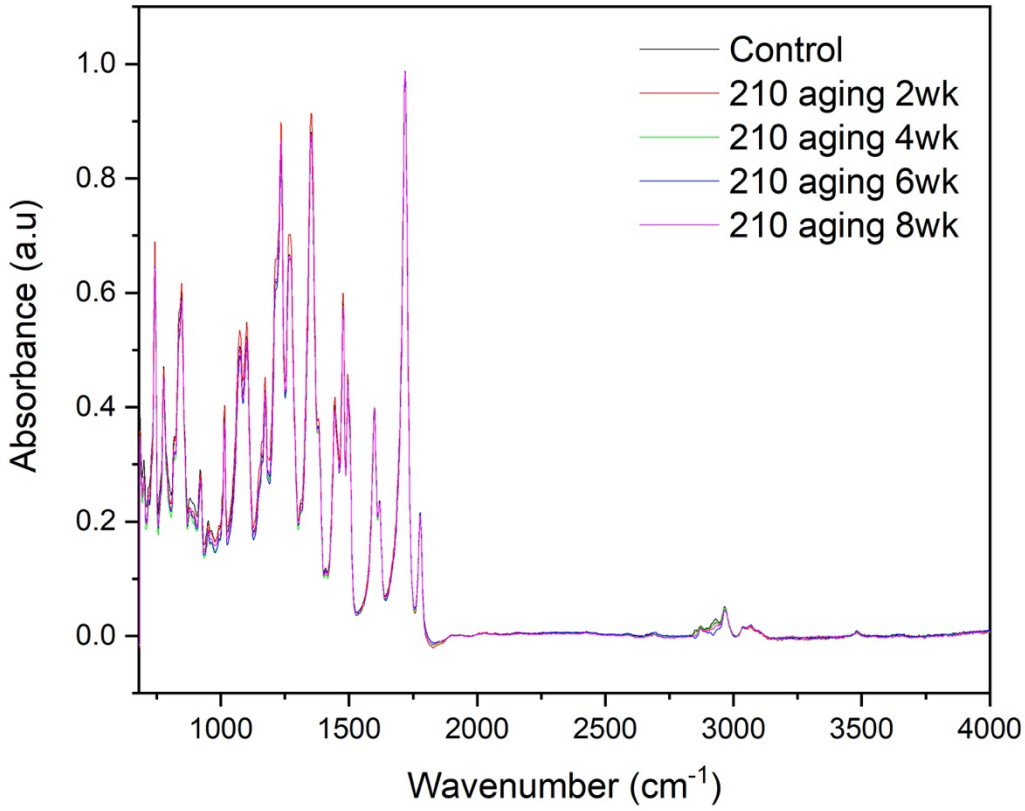

Figure 6: FTIR spectroscopy spectra at different thermal aging times (0, 2, 4, 6 and 8 weeks) for an aging temperature of 210 °C

The main FTIR peaks of PEI have been documented previously by Amancio-Filho et al.[8] The location of these peaks, along with the corresponding vibrations of chemical bonds in the PEI molecule are shown in Table 3. This includes aryl-ether-aryl, propylidene, C-N stretching, C-H stretching, C=C vibration, and C=O (in the imide group).

Table 3: FTIR spectroscopy peaks of PEI and corresponding vibrations of chemical bonds. Adapted from [8].

Wavenumber (cm^{-1})	Vibrations of chemical bonds
1014, 1074, 1269, 1234	Ar-O-Ar (aryl ether aryl) [41,42]
1172	iso propylidene [43]
1224	C-O absorption [44]
1351, 1215	C-N stretching [45,46]
2965, 2873	C-H stretching [47,48]
1618, 1600,1494, 1444	C=C vibration [49–51]
1777, 1718	C=O group(s) in imide [51,52]

In general, FTIR characterization in various polymer aging/degradation studies has been implemented using the "peak area" comparison.[53–57] Monitoring the peak area after subtracting the background and eventually deconvoluting overlapping peaks is an established method to quantify subtle chemical changes in a given functional group, such as degradation,[53] carbonyl formation,[54] conversion of polymerization,[56] or grafting process[57]. The area of the peak of interest is normalized by the area of a peak unaffected by the degradation process.[55]

Figure 7 shows an example of the determination of the peak area for the peak at 1215 cm^{-1}, which corresponds to the C-N stretching in the phthalimide ring. The peak area was calculated after deconvolution of the three overlapping peaks at 1215, 1224, and 1234 cm^{-1}. The 1224 cm^{-1} and 1234 cm^{-1} peaks are from C-O adsorption[44] and Ar-O-Ar bonds[41,42], respectively, and were found in all conditions. The variation in the 1215 cm^{-1} peak area as a function of the aging time at 210 °C is shown in Figure 8. The mean values of the peak areas did not appear to change much between 0 and 2 weeks (336 h) of aging. On the other hand, the peak areas between 4 and 8 weeks of aging are statistically different from the values for the control and 2 weeks of aging. The reduction in the peak area between 2 and 6 weeks (336 and 1008 h) of aging is equal to 15%. This decrease in the FTIR peak area corresponding to the C-N stretching in the phthalimide ring can potentially be attributed to chain scission in the C-N bond resulting from the thermal aging process.[15]

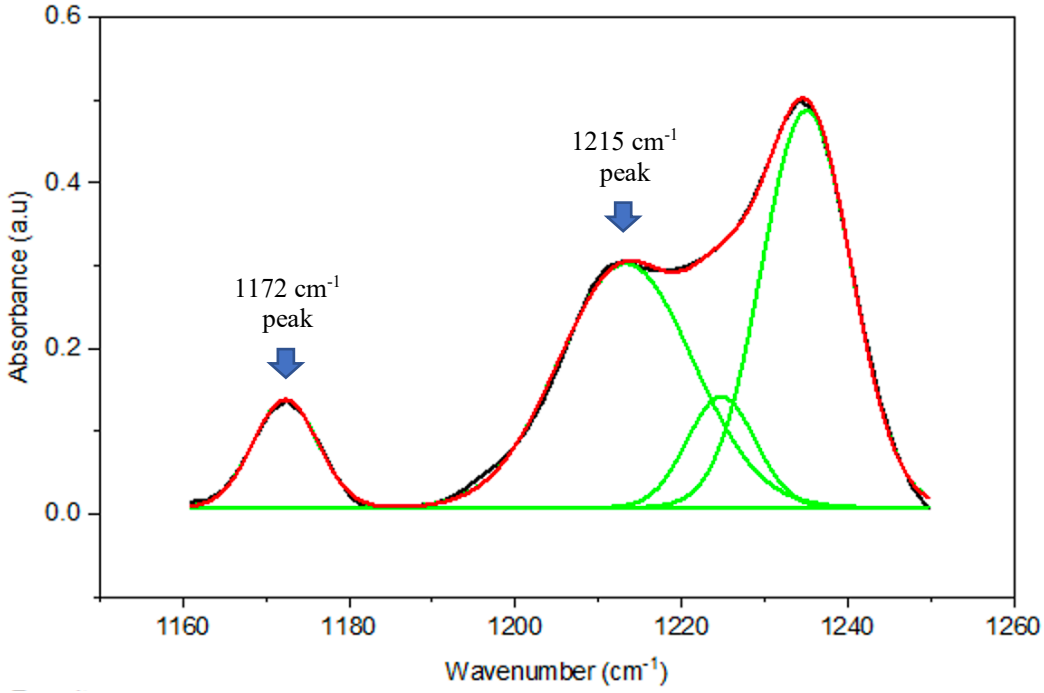

Figure 7: Peak deconvolution for the isopropylidene (1172 cm^{-1}) and C-N stretching (1215 cm^{-1}) peak area determination

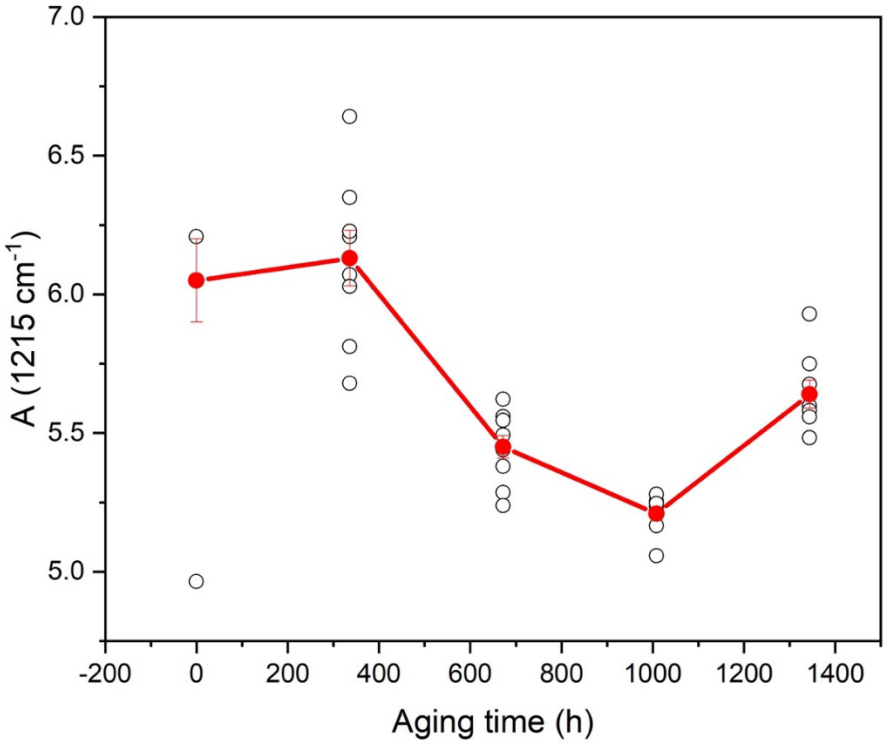

Figure 8: Variation in the 1215 cm^{-1} peak area associated to C-N stretching in the phthalimide ring as a function of the aging time at 210 °C. The open circles correspond to the values for each individual sample.

The variation in the peak area as a function of the aging time at 210 °C for the 1172 cm^{-1} peak associated with the propylidene group is illustrated in Figure 9. The mean values of the peak areas show a continuous decrease with aging time. Based on the statistical analysis, the peak areas for the control condition and at 2 weeks of aging have a statistically significant difference with the conditions at 6 and 8 weeks of aging (detail post-hoc analysis included in supporting information section S8). This result can be attributed to the occurrence of chain scission of the propylidene group during thermal aging, in agreement with the conclusion of Carroccio et al. who investigated the thermal degradation mechanisms of PEI by pyrolysis.[15]

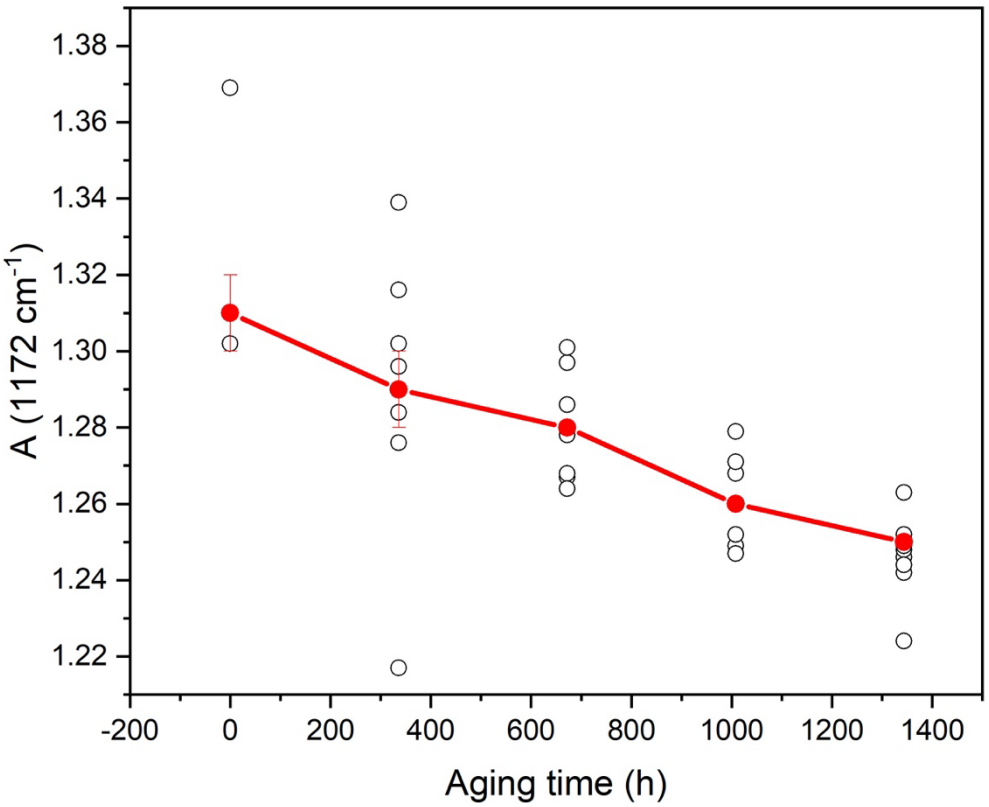

Figure 9: Variation in the 1172 cm^{-1} peak area associated to the propylidene group as a function of the aging time at 210 °C. The open circles correspond to the values for each individual sample.

The changes in the FTIR peak areas corresponding to the phthalimide and propylidene groups as a result of thermal aging are in agreement with the results of Musto et al.[58] These results point towards two specific mechanisms for the thermal aging of PEI conducted in our study:

- N-H transfer from phthalimide ring (identified as R_5 in Figure 10);
- C-H transfer after disproportionation in propylidene group (identified as R_3 in Figure 10).

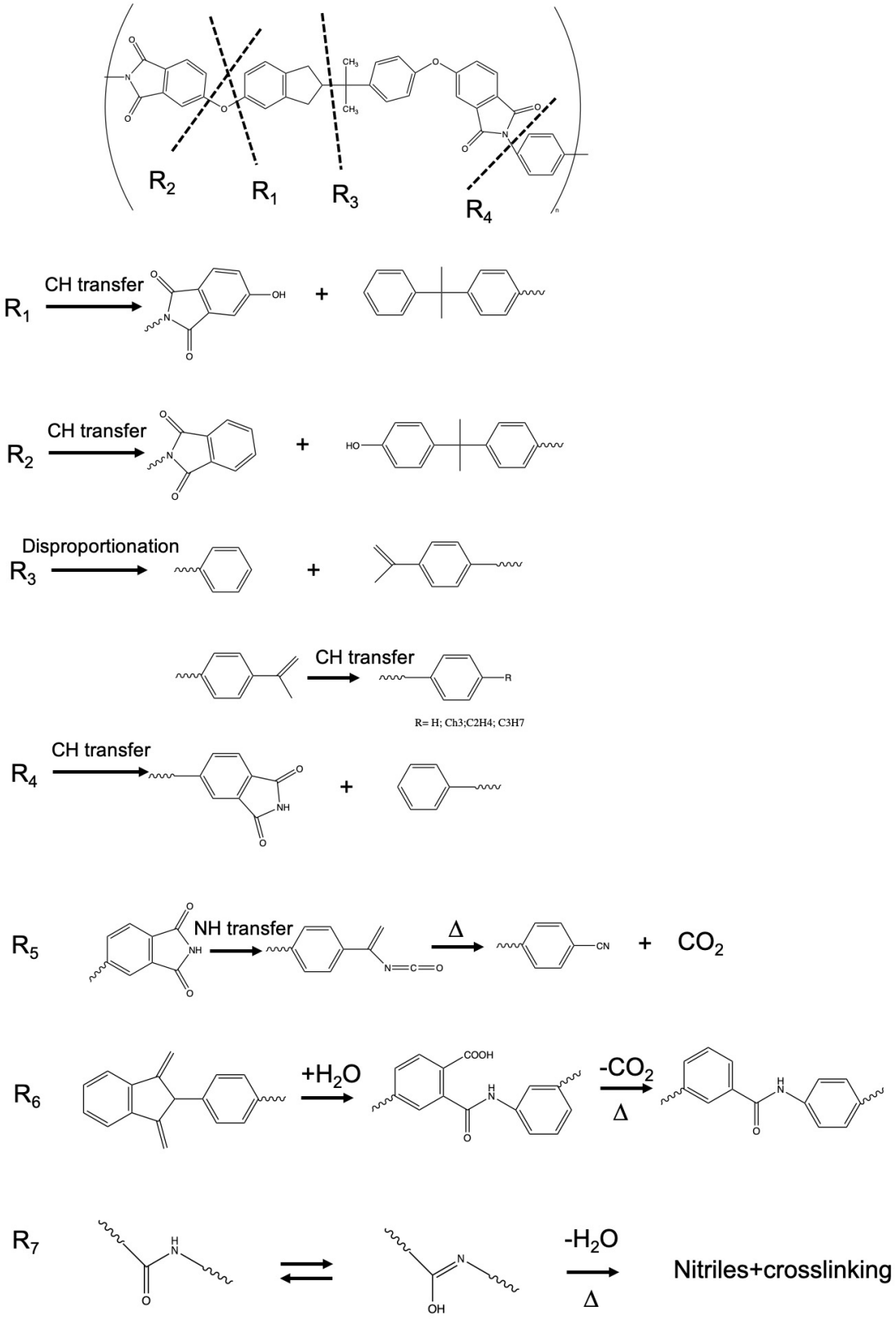

Figure 10: Possible mechanisms of thermal chain scission of PEI.[15]

3.4. Surface characterization of PEI

The influence of thermal aging on polymer surfaces has been studied in various polymers and resins, and can result for example in micro-crack formation, surface cracking, or change in surface roughness.[59–61] In order to investigate the effect of thermal aging on the surface of PEI samples, FE-SEM images were taken at different aging times and temperatures. Figure 11 shows examples of results obtained for the control samples (Figure 11a), after 12 weeks of aging at 190 °C (Figure 11b) and 200 °C (Figure 11c), and after 8 weeks of aging at 210 °C (Figure 11d). A difference between the surface of the control and aged PEI samples is the emergence of cracks on the surface of the thermally aged PEI samples. The condition corresponding to 12 weeks of aging at 190 °C (Figure 11b) can be associated with a few sub-micron cracks and some non-uniform areas. With 12 weeks of aging at 200 °C (Figure 11c), both the surface area that is occupied by the crack-dense zones and the number of these crack-dense zones have increased. After 8 weeks of aging at 210 °C (Figure 11d), sub-micron cracks are visible over the entire surface of the SEM image.

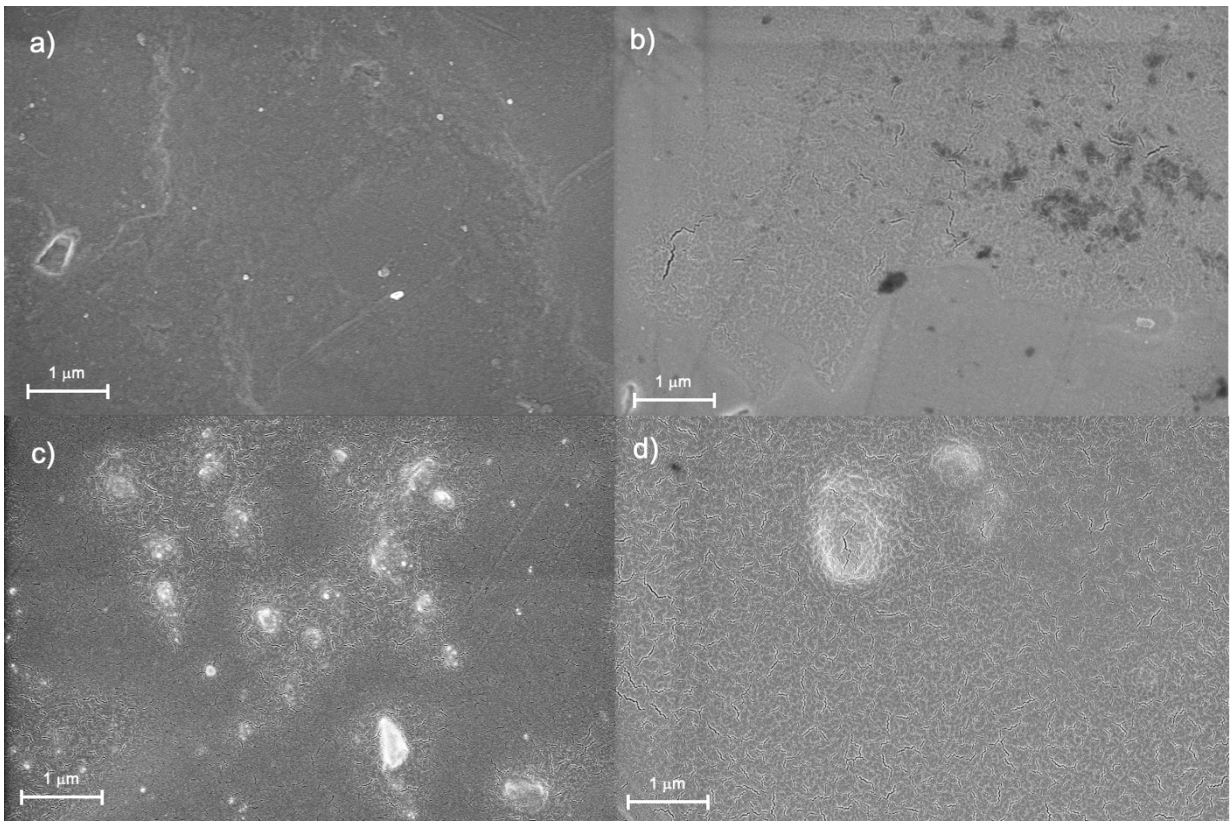

Figure 11: FE-SEM image of the surface of PEI specimens, a) control, b) aged at 190 °C for 12 weeks, c) aged at 200 °C for 12 weeks, and d) aged at 210 °C for 8 weeks.

The surface area occupied by the cracks was quantified for the different thermal aging times and temperatures using the FE-SEM images and ImageJ (e.g.: Supporting Information Figure S6). Figure 12 illustrates the variation of the crack area (%) as a function of the aging time for the three aging temperatures. The crack area increases both with aging time and temperature. This suggests that chain scission occurs during thermal aging, causing some areas to weaken. When the specimens are removed from the oven after the aging period, the cooling from the aging temperature (190 °C to 210 °C) to room temperature generates thermal stress. As this thermal stress is applied to areas weakened by thermal aging, cracks may form and propagate.[62]

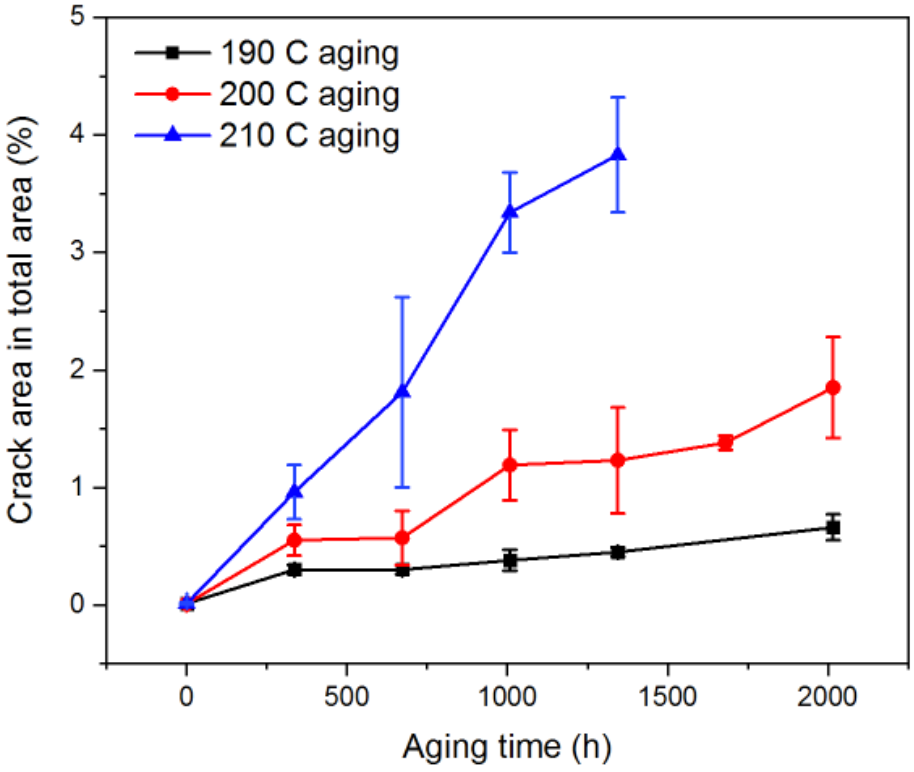

Figure 7: Crack density in the 222.1 μm^2 area of thermally aged PEI as a function of aging time at different aging temperatures.

The surface roughness of the PEI samples before and after aging at the different conditions was also characterized using AFM. In the literature, authors have reported that the surface roughness of polymers (including polycarbonate and polyester) increases after thermal aging because of added matter or the formation of holes/cracks on the surface during aging.[63] In our

case, the control PEI film exhibited a unique pattern associated with the manufacturing process (Figure 13). Figure 14 displays the 3D AFM images of the surface of control PEI specimens and those after 8 weeks of aging at 190 °C, 200 °C, and 210 °C. The control PEI film has a surface roughness (R_q) of 0.16 ± 0.01 μm. After thermal aging, the surface roughness was found to decrease (Table 4).

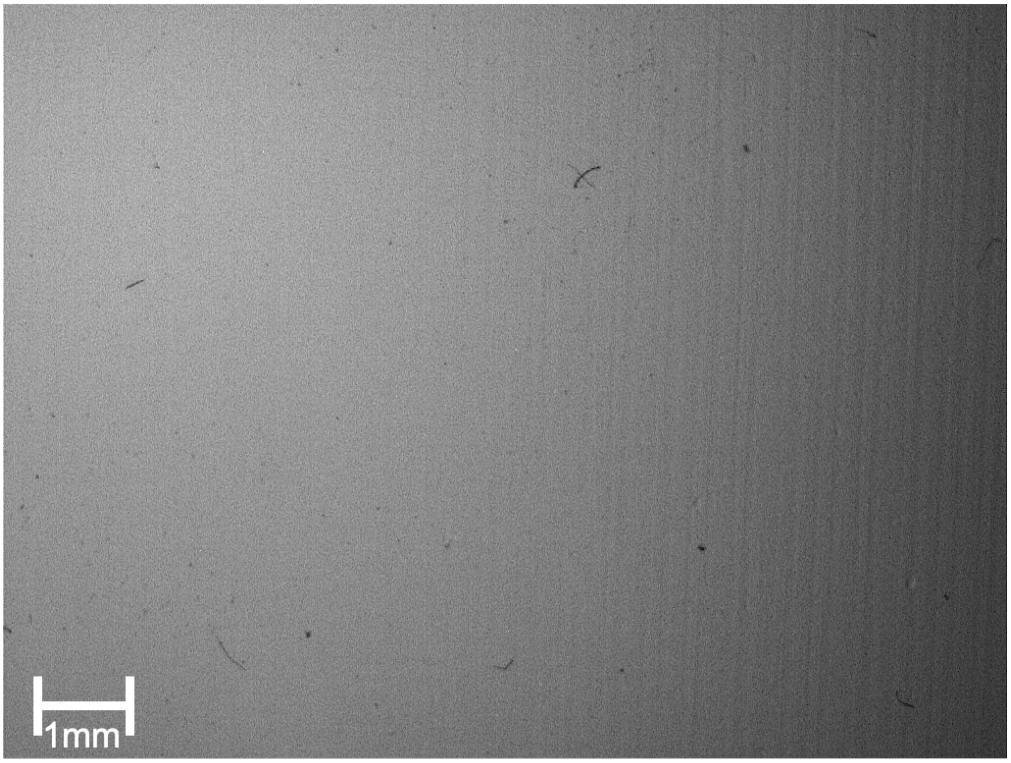

Figure 8: Optical microscope image of the control PEI film.

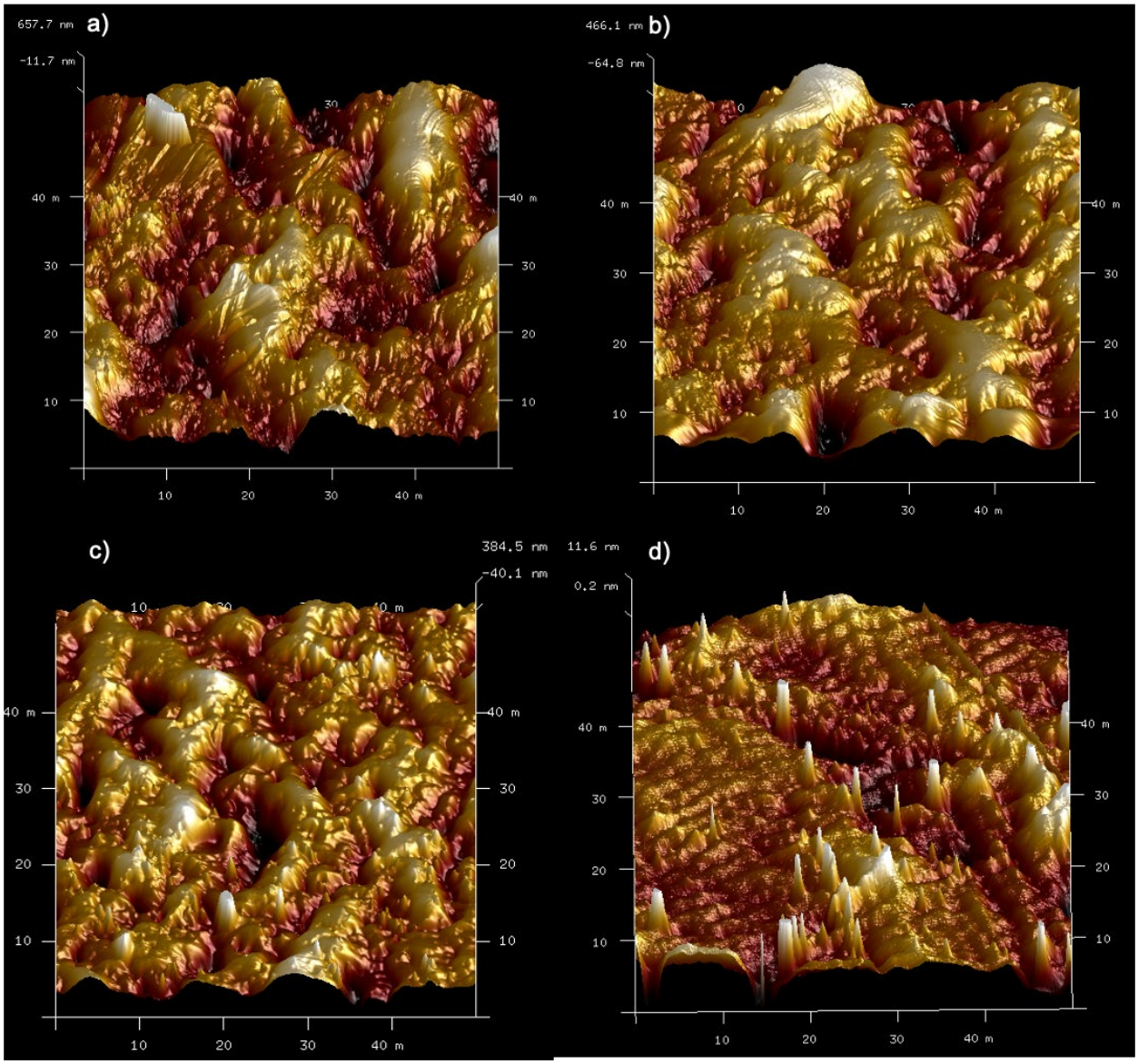

Figure 9: 3D AFM images of the PEI film surface in the a) control condition and after aging for 8 weeks at different temperatures b) 190 °C, c) 200 °C, d) 210 °C.

Table 4: Surface roughness of the unaged and thermally aged PEI film samples

Aging temperature/time	Surface roughness (R_q)
Control (unaged)	0.16 ± 0.01 µm
190 °C/8 weeks	0.16 ± 0.01 µm
200 °C/8 weeks	0.12 ± 0.01 µm
210 °C/8 weeks	0.03 ± 0.01 µm

A visible change in the PEI film was also observed. The neat PEI film was initially semi-transparent (Figure 15a). It became gradually transparent to visible light after thermal aging (Figure 15 b-d).

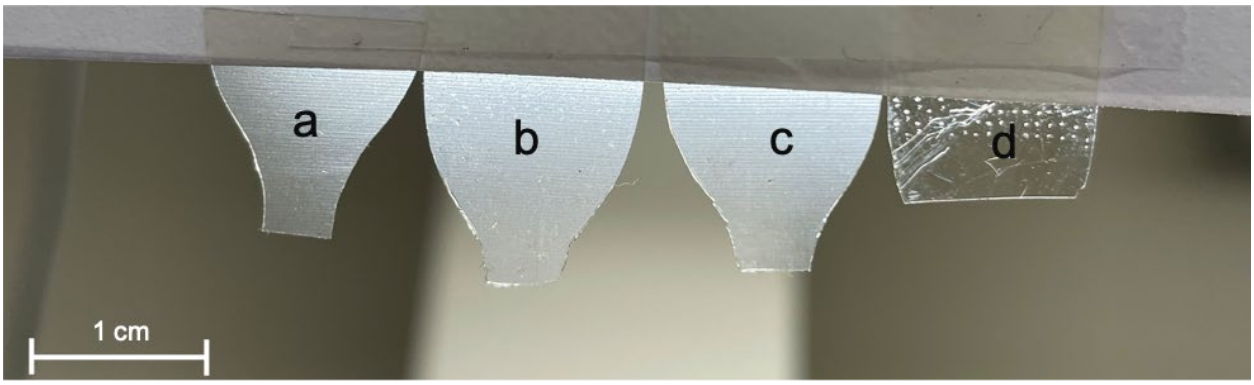

Figure 10: Change in the PEI film transparency after thermal aging for 8 weeks at different temperatures. a) control, b) 190 °C, c) 200 °C, and d) 210 °C.

4. Conclusions

The accelerated thermal aging behavior of PEI was investigated. Specimens taken from a PEI film were exposed to three different temperatures (190 °C, 200 °C, and 210 °C) in air for times of up to 16 weeks depending on the aging temperature. The FTIR analysis showed that chemical bonds in PEI were consumed due to chain scission. The thermal aging was also associated with the formation of microcracks on the surface of the PEI specimens. The surface area occupied by these cracks increased with longer aging times and higher aging temperatures. An irreversible deformation was also observed as a result of thermal aging, reducing the PEI film roughness and increasing its transparency to visible light.

In terms of mechanical behavior, the aged PEI showed changes in UTS. The first phase of the thermal aging resulted in an increase in UTS due to crosslinking reactions. For shorter aging times, this crosslinking resulted both in an increase in the UTS and in the glass transition temperature (crosslinking reactions reduce the mobility of the polymer network). For longer aging times and higher aging temperatures, the UTS of PEI underwent a decrease due to chain scission. Using the UTS data, a master curve was constructed based on the application of the TTS principle. The shift factors yielded a value of the activation energy of 112 kJ mol^{-1}. This value is similar to values of activation energy reported for fire-protective fabric blends used as the outer shell in firefighter protective clothing, with for instance an activation energy of 111 kJ mol^{-1} for a 60/40 Kevlar®/PBI fabric and of 113 kJ mol^{-1} for a 60/40 Kevlar®/Nomex® IIIA (93% Nomex®, 5% Kevlar®, 2% carbon fibers) fabric.

As PEI was shown to have a similar activation energy upon thermal aging as many fire-protective materials and display detectable changes in both strength and surface properties, changes in the properties of this material could potentially be used to track exposure to high temperature conditions. PEI films therefore present an interesting option for use as the sacrificial polymer layer for the development of a thermal aging end-of-life sensor for fire-protective fabrics. Because high performance fibers used in fire-protective clothing often age without visible signs, such end-of-life sensors are critical to monitor the effect that the long-term exposure of fire-protective clothing to service conditions has on their performance.

Supporting Information

Supporting information is available from Supporting Information section at the end of this article.

Acknowledgements

This project has received a funding from the Natural Sciences and Engineering Research Council of Canada (NSERC) (STPGP 521866 - 18). The authors also want to acknowledge the support provided by the Protective Clothing and Equipment Research Facility (PCERF) and Dr. Jane Batcheller in the Human Ecology Department, the Analytical and Instrumentation Laboratory and Mr. Wayne Moffat in the Chemistry Department, and nanoFAB in the Faculty of Engineering at the University of Alberta.

References

1. Bhowmik, S.; Bonin, H. W.; Bui, V. T.; Weir, R. D. Modification of High-Performance Polymer Composite through High-Energy Radiation and Low-Pressure Plasma for Aerospace and Space Applications. *J. Appl. Polym. Sci.* **2006**, *102* (2), 1959–1967. https://doi.org/10.1002/app.24230.
2. Serfaty, I. W. Polyetherimide: A Versatile, Processable Thermoplastic BT - Polyimides: Synthesis, Characterization, and Applications. Volume 1; Mittal, K. L., Ed.; Springer US: Boston, MA, 1984; pp 149–161. https://doi.org/10.1007/978-1-4615-7637-2_10.
3. Liu, S.; Fifield, L. S.; Bowler, N. Aging Mechanisms and Nondestructive Aging Indicator of Filled Cross-Linked Polyethylene (XLPE) Exposed to Simultaneous Thermal and Gamma Radiation. In *Minerals, Metals and Materials Series*; 2018; pp 65–75. https://doi.org/10.1007/978-3-319-68454-3_6.
4. Searle, O. B.; Pfeiffer, R. H. Victrex® Poly(Ethersulfone) (PES) and Victrex® Poly(Etheretherketone) (PEEK). *Polym. Eng. Sci.* **1985**, *25* (8), 474–476. https://doi.org/10.1002/pen.760250808.
5. Macocinschi, D.; Grigoriu, A.; Filip, D. Aromatic Polysulfones for Flame Retardancy. *Eur. Polym. J.* **2002**, *38* (5), 1025–1031. https://doi.org/10.1016/S0014-3057(01)00253-1.
6. Hill, H. W.; Brady, D. G. Properties, Environmental Stability, and Molding Characteristics of Polyphenylene Sulfide. *Polym. Eng. Sci.* **1976**, *16* (12), 831–835. https://doi.org/10.1002/pen.760161211.
7. McKeen, L. W. Polyimides. In *The Effect of Long Term Thermal Exposure on Plastics and Elastomers*; Elsevier: Oxford, 2014; pp 117–137. https://doi.org/10.1016/B978-0-323-22108-5.00006-0.
8. Amancio-Filho, S. T.; Roeder, J.; Nunes, S. P.; dos Santos, J. F.; Beckmann, F. Thermal Degradation of Polyetherimide Joined by Friction Riveting (FricRiveting). Part I: Influence of Rotation Speed. *Polym. Degrad. Stab.* **2008**, *93* (8), 1529–1538. https://doi.org/https://doi.org/10.1016/j.polymdegradstab.2008.05.019.
9. Yilmaz, T.; Sinmazcelik, T. Effects of Hydrothermal Aging on Glass–Fiber/Polyetherimide (PEI) Composites. *J. Mater. Sci.* **2010**, *45* (2), 399–404. https://doi.org/10.1007/s10853-009-3954-1.
10. Tzounis, L.; Hegde, M.; Liebscher, M.; Dingemans, T.; Pötschke, P.; Paipetis, A. S.;

Zafeiropoulos, N. E.; Stamm, M. All-Aromatic SWCNT-Polyetherimide Nanocomposites for Thermal Energy Harvesting Applications. *Compos. Sci. Technol.* **2018**, *156*, 158–165. https://doi.org/https://doi.org/10.1016/j.compscitech.2017.12.030.

11. GE Plastics. ULTEM® PEI Resin Product Guide http://www-eng.lbl.gov/~shuman/NEXT/CURRENT_DESIGN/EP/ULTEMProductBrochure.pdf (accessed Apr 26, 2020).
12. Long Jr., E. R.; Collins, W. D. The Effects of Fluids in the Aircraft Environment on a Polyetherimide. *Polym. Eng. Sci.* **1988**, *28* (12), 823–828. https://doi.org/https://doi.org/10.1002/pen.760281208.
13. Ehrenstein, G. W.; Pongratz, S. Principles of Aging. In *Resistance and Stability of Polymers*; Carl Hanser Verlag GmbH & Co. KG: München, 2013; pp 1–138. https://doi.org/10.3139/9783446437098.001.
14. Zhao, J.; Yang, R.; Iervolino, R.; Barbera, S. Investigation of Crosslinking in the Thermooxidative Aging of Nitrile-Butadiene Rubber. *J. Appl. Polym. Sci.* **2015**, *132* (3), 41319 (1-5). https://doi.org/10.1002/app.41319.
15. Carroccio, S.; Puglisi, C.; Montaudo, G. Thermal Degradation Mechanisms of Polyetherimide Investigated by Direct Pyrolysis Mass Spectrometry. *Am. Chem. Soc. Polym. Prepr. Div. Polym. Chem.* **2000**, *200* (10), 2345–2355.
16. Lisa, G.; Hamciuc, C.; Hamciuc, E.; Tudorachi, N. Thermal and Thermo-Oxidative Stability and Probable Degradation Mechanism of Some Polyetherimides. *J. Anal. Appl. Pyrolysis* **2016**, *118*, 144–154. https://doi.org/https://doi.org/10.1016/j.jaap.2016.01.012.
17. Courvoisier, E.; Bicaba, Y.; Colin, X. Multi-Scale and Multi-Technical Analysis of the Thermal Degradation of Poly(Ether Imide). *Polym. Degrad. Stab.* **2018**, *147*, 177–186. https://doi.org/https://doi.org/10.1016/j.polymdegradstab.2017.12.002.
18. Batista, N. L.; Costa, M. L.; Iha, K.; Botelho, E. C. Thermal Degradation and Lifetime Estimation of Poly(Ether Imide)/Carbon Fiber Composites. *J. Thermoplast. Compos. Mater.* **2015**, *28* (2), 265–274. https://doi.org/10.1177/0892705713484740.
19. ISO. *ISO 527:2012 Plastics — Determination of Tensile Properties*; 2006.
20. Bourbigot, S.; Flambard, X. Heat Resistance and Flammability of High Performance Fibres: A Review. *Fire Mater.* **2002**. https://doi.org/10.1002/fam.799.
21. Abbasi, H.; Antunes, M.; Velasco, J. Polyetherimide Foams Filled with Low Content of

Graphene Nanoplatelets Prepared by ScCO2 Dissolution. *Polymers (Basel).* **2019**, *11* (2), 328. https://doi.org/10.3390/polym11020328.

22. Wu, C. S.; Liu, Y. L.; Chiu, Y. C.; Chiu, Y. S. Thermal Stability of Epoxy Resins Containing Flame Retardant Components: An Evaluation with Thermogravimetric Analysis. *Polym. Degrad. Stab.* **2002**, *78* (1), 41–48. https://doi.org/https://doi.org/10.1016/S0141-3910(02)00117-9.
23. Rychlý, J.; Rychlá, L. Modelling of Heat Release Rate-Time Curves from Cone Calorimeter for Burning of Polymers with Intumescence Additives. *Polym. Degrad. Stab.* **1996**, *54* (2–3), 249–254. https://doi.org/10.1016/S0141-3910(96)00050-X.
24. Menczel, J. D.; Judovits, L.; Prime, R. B.; Bair, H. E.; Reading, M.; Swier, S. Differential Scanning Calorimetry (DSC). *Thermal Analysis of Polymers*. April 3, 2009, pp 7–239. https://doi.org/https://doi.org/10.1002/9780470423837.ch2.
25. Chen, X. Y.; Romero, A.; Paton-Carrero, A.; Lavin-Lopez, M. P.; Sanchez-Silva, L.; Valverde, J. L.; Kaliaguine, S.; Rodrigue, D. Functionalized Graphene–Reinforced Foams Based on Polymer Matrices. In *Functionalized Graphene Nanocomposites and their Derivatives*; Elsevier, 2019; pp 121–155. https://doi.org/10.1016/B978-0-12-814548-7.00007-6.
26. Banks, L.; Ellis, B. The Glass Transition Temperatures of Highly Crosslinked Networks: Cured Epoxy Resins. *Polymer (Guildf).* **1982**, *23* (10), 1466–1472. https://doi.org/https://doi.org/10.1016/0032-3861(82)90246-4.
27. Bicerano, J.; Sammler, R. L.; Carriere, C. J.; Seitz, J. T. Correlation between Glass Transition Temperature and Chain Structure for Randomly Crosslinked High Polymers. *J. Polym. Sci. Part B Polym. Phys.* **1996**, *34* (13), 2247–2259. https://doi.org/https://doi.org/10.1002/(SICI)1099-0488(19960930)34:13<2247::AID-POLB14>3.0.CO;2-5.
28. Glatz-Reichenbach, J. K. W.; Sorriero, L.; Fitzgerald, J. J. Influence of Crosslinking on the Molecular Relaxation of an Amorphous Copolymer Near Its Glass-Transition Temperature. *Macromolecules* **1994**, *27* (6), 1338–1343. https://doi.org/10.1021/ma00084a010.
29. Tcharkhtchi, A.; Farzaneh, S.; Abdallah-Elhirtsi, S.; Esmaeillou, B.; Nony, F.; Baron, A. Thermal Aging Effect on Mechanical Properties of Polyurethane. *Int. J. Polym. Anal.*

Charact. **2014**, *19* (7), 571–584. https://doi.org/10.1080/1023666X.2014.932644.

30. Sang, L.; Wang, C.; Wang, Y.; Wei, Z. Thermo-Oxidative Ageing Effect on Mechanical Properties and Morphology of Short Fibre Reinforced Polyamide Composites – Comparison of Carbon and Glass Fibres. *RSC Adv.* **2017**, *7* (69), 43334–43344. https://doi.org/10.1039/C7RA07884F.
31. Yang, L.; Ohki, Y.; Hirai, N.; Hanada, S. Aging of Poly(Ether Ether Ketone) by Heat and Gamma Rays — Its Degradation Mechanism and Effects on Mechanical, Dielectric and Thermal Properties. *Polym. Degrad. Stab.* **2017**, *142*, 117–128. https://doi.org/10.1016/j.polymdegradstab.2017.06.002.
32. Mecheri, Y.; Boukezzi, L.; Boubakeur, A.; Lallouani, M. Dielectric and Mechanical Behavior of Cross-Linked Polyethylene under Thermal Aging. In *2000 Annual Report Conference on Electrical Insulation and Dielectric Phenomena (Cat. No.00CH37132)*; IEEE, 2000; Vol. 2, pp 560–563. https://doi.org/10.1109/CEIDP.2000.884022.
33. Sirisinha, C.; Sae-Oui, P.; Guaysomboon, J. Mechanical Properties, Oil Resistance, and Thermal Aging Properties in Chlorinated Polyethylene/Natural Rubber Blends. *J. Appl. Polym. Sci.* **2002**, *84* (1), 22–28. https://doi.org/10.1002/app.10171.
34. Parkman, L. E. Viscoelastic Effects On A Polyetherimide Cylinder With Constant Radial Deformation, THE UNIVERSITY OF TEXAS AT ARLINGTON, 2015.
35. Yin, W.; Xie, Z.; Yin, Y.; Yi, J.; Liu, X.; Wu, H.; Wang, S.; Xie, Y.; Yang, Y. Aging Behavior and Lifetime Prediction of PMMA under Tensile Stress and Liquid Scintillator Conditions. *Adv. Ind. Eng. Polym. Res.* **2019**, *2* (2), 82–87. https://doi.org/10.1016/j.aiepr.2019.04.002.
36. Anh, T. H.; Vu-Khanh, T. Effects of Thermal Aging on Fracture Performance of Polychloroprene. *J. Mater. Sci.* **2005**, *40* (19), 5243–5248. https://doi.org/10.1007/s10853-005-4418-x.
37. Bernstein, R.; Gillen, K. T. Nylon 6.6 Accelerating Aging Studies: II. Long-Term Thermal-Oxidative and Hydrolysis Results. *Polym. Degrad. Stab.* **2010**, *95* (9), 1471–1479. https://doi.org/10.1016/j.polymdegradstab.2010.06.018.
38. Arrieta, C.; David, E.; Dolez, P.; Vu-Khanh, T. Thermal Aging of a Blend of High-Performance Fibers. *J. Appl. Polym. Sci.* **2009**, *115* (5), 3031–3039.
39. Dolez, P. I.; Tomer, N. S.; Malajati, Y. A Quantitative Method to Compare the Effect of

Thermal Aging on the Mechanical Performance of Fire Protective Fabrics. *J. Appl. Polym. Sci.* **2019**, *136* (6), 47045. https://doi.org/10.1002/app.47045.

40. Zhang, Y.-Y.; Sun, Z.; Li, Y.-Q.; Huang, P.; Chen, Q.; Fu, S.-Y. Tensile Creep Behavior of Short-Carbon-Fiber Reinforced Polyetherimide Composites. *Compos. Part B Eng.* **2021**, *212*, 108717. https://doi.org/https://doi.org/10.1016/j.compositesb.2021.108717.
41. Jiao, L.; Xiao, H.; Wang, Q.; Sun, J. Thermal Degradation Characteristics of Rigid Polyurethane Foam and the Volatile Products Analysis with TG-FTIR-MS. *Polym. Degrad. Stab.* **2013**, *98* (12), 2687–2696. https://doi.org/10.1016/j.polymdegradstab.2013.09.032.
42. Romero, A. I.; Parentis, M. L.; Habert, A. C.; Gonzo, E. E. Synthesis of Polyetherimide/Silica Hybrid Membranes by the Sol–Gel Process: Influence of the Reaction Conditions on the Membrane Properties. *J. Mater. Sci.* **2011**, *46* (13), 4701–4709. https://doi.org/10.1007/s10853-011-5380-4.
43. Wan Nurul Huda, W. Z.; Ahmad, M. A. Effect of the Pyrolysis Soaking Time on CO2 Separation of Polyetherimide/Polyethylene Glycol-Based CMS Membranes. In *Developments in Sustainable Chemical and Bioprocess Technology*; Springer US: Boston, MA, 2013; pp 329–335. https://doi.org/10.1007/978-1-4614-6208-8_39.
44. Ding, S.; Zou, B.; Wang, P.; Ding, H. Effects of Nozzle Temperature and Building Orientation on Mechanical Properties and Microstructure of PEEK and PEI Printed by 3D-FDM. *Polym. Test.* **2019**, *78*, 105948. https://doi.org/https://doi.org/10.1016/j.polymertesting.2019.105948.
45. Shah, S. S. A.; Nasir, H.; Saboor, A. Improved Dielectric Properties of Polyetherimide and Polyaniline-Coated Few-Layer Graphene Based Nanocomposites. *J. Mater. Sci. Mater. Electron.* **2018**, *29* (1), 402–411. https://doi.org/10.1007/s10854-017-7929-8.
46. Reddy, K. R.; Sin, B. C.; Yoo, C. H.; Sohn, D.; Lee, Y. Coating of Multiwalled Carbon Nanotubes with Polymer Nanospheres through Microemulsion Polymerization. *J. Colloid Interface Sci.* **2009**, *340* (2), 160–165. https://doi.org/10.1016/j.jcis.2009.08.044.
47. JIANG, X.; Ellis, N.; ZHONG, Z. Characterization of Pyrolytic Lignin Extracted from Bio-Oil. *Chinese J. Chem. Eng.* **2010**, *18* (6), 1018–1022. https://doi.org/10.1016/S1004-9541(09)60162-2.
48. Saliba, J. B.; Faraco, A. A. G.; Yoshida, M. I.; Vasconcelos, W. L. de; Silva-Cunha, A.

da; Mansur, H. S. Development and Characterization of an Intraocular Biodegradable Polymer System Containing Cyclosporine-A for the Treatment of Posterior Uveitis. *Mater. Res.* **2008**, *11* (2), 207–211. https://doi.org/10.1590/S1516-14392008000200016.

49. Kurdi, J.; Kumar, A. Structuring and Characterization of a Novel Highly Microporous PEI/BMI Semi-Interpenetrating Polymer Network. *Polymer (Guildf).* **2005**, *46* (18), 6910–6922. https://doi.org/10.1016/j.polymer.2005.06.057.
50. Rajagopalan, M.; Oh, I.-K. Fullerenol-Based Electroactive Artificial Muscles Utilizing Biocompatible Polyetherimide. *ACS Nano* **2011**, *5* (3), 2248–2256. https://doi.org/10.1021/nn103521g.
51. Pitchan, M. K.; Bhowmik, S.; Balachandran, M.; Abraham, M. Effect of Surface Functionalization on Mechanical Properties and Decomposition Kinetics of High Performance Polyetherimide/MWCNT Nano Composites. *Compos. Part A Appl. Sci. Manuf.* **2016**, *90*, 147–160. https://doi.org/10.1016/j.compositesa.2016.06.025.
52. Tunckol, M.; Hernandez, E. Z.; Sarasua, J.-R.; Durand, J.; Serp, P. Polymerized Ionic Liquid Functionalized Multi-Walled Carbon Nanotubes/Polyetherimide Composites. *Eur. Polym. J.* **2013**, *49* (12), 3770–3777. https://doi.org/10.1016/j.eurpolymj.2013.08.007.
53. Partini, M.; Pantani, R. FTIR Analysis of Hydrolysis in Aliphatic Polyesters. *Polym. Degrad. Stab.* **2007**, *92* (8), 1491–1497. https://doi.org/https://doi.org/10.1016/j.polymdegradstab.2007.05.009.
54. Bauer, D. R.; Gerlock, J. L.; Mielewski, D. F.; Paputa Peck, M. C.; Carter, R. O. Photo-Stabilization and Photo-Degradation in Organic Coatings Containing a Hindered Amine Light Stabilizer: Part IV—Photo-Initiation Rates and Photo-Oxidation Rates in Unstabilized Coatings. *Polym. Degrad. Stab.* **1990**, *27* (3), 271–284. https://doi.org/https://doi.org/10.1016/0141-3910(90)90011-U.
55. Zhang, Y.; Maxted, J.; Barber, A.; Lowe, C.; Smith, R. The Durability of Clear Polyurethane Coil Coatings Studied by FTIR Peak Fitting. *Polym. Degrad. Stab.* **2013**, *98* (2), 527–534. https://doi.org/https://doi.org/10.1016/j.polymdegradstab.2012.12.003.
56. Rydholm, A. E.; Held, N. L.; Bowman, C. N.; Anseth, K. S. Gel Permeation Chromatography Characterization of the Chain Length Distributions in Thiol−Acrylate Photopolymer Networks. *Macromolecules* **2006**, *39* (23), 7882–7888. https://doi.org/10.1021/ma060858u.

57. Nugroho, R. W. N.; Odelius, K.; Höglund, A.; Albertsson, A.-C. The Nature of Polymer Grafts and Substrate Shape on the Surface Degradation of Poly(l-Lactide). *J. Appl. Polym. Sci.* **2015**, *132* (47). https://doi.org/https://doi.org/10.1002/app.42736.
58. Musto, P.; Karasz, F. E.; MacKnight, W. J. Fourier Transform Infra-Red Spectroscopy on the Thermo-Oxidative Degradation of Polybenzimidazole and of a Polybenzimidazole/Polyetherimide Blend. *Polymer (Guildf).* **1993**, *34* (14), 2934–2945. https://doi.org/10.1016/0032-3861(93)90618-K.
59. Meftah, H.; Tamboura, S.; Fitoussi, J.; BenDaly, H.; Tcharkhtchi, A. Thermal Aging Influence on the Damage Mechanisms of Fully Recycled Composite-reinforced Polypropylene/Polyethylene Blend. *Polym. Compos.* **2019**, *40* (8), 3342–3350. https://doi.org/10.1002/pc.25194.
60. Bowles, K. J.; Jayne, D.; Leonhardt, T. A. Isothermal Aging Effects on PMR-15 Resin. *NASA Tech. Memo. 105648* **1993**, 1–20.
61. Suresh, B.; Maruthamuthu, S.; Khare, A.; Palanisamy, N.; Muralidharan, V. S.; Ragunathan, R.; Kannan, M.; Pandiyaraj, K. N. Influence of Thermal Oxidation on Surface and Thermo-Mechanical Properties of Polyethylene. *J. Polym. Res.* **2011**, *18* (6), 2175–2184. https://doi.org/10.1007/s10965-011-9628-0.
62. Awaja, F.; Zhang, S.; Tripathi, M.; Nikiforov, A.; Pugno, N. Cracks, Microcracks and Fracture in Polymer Structures: Formation, Detection, Autonomic Repair. *Prog. Mater. Sci.* **2016**, *83*, 536–573. https://doi.org/10.1016/j.pmatsci.2016.07.007.
63. Wang, W.; He, D.; Yang, K.; Liu, S.; Song, S.; Yi, D. Research of the Thermal Aging Mechanism of Polycarbonate and Polyester Film. *e-Polymers* **2017**, *17* (1), 45–56. https://doi.org/10.1515/epoly-2016-0179.

Supporting Information

S1. Materials and specimen preparation

Each specimen was labelled with a code "A-a-#", where "A" corresponds to the film number (A-H), "a" indicates the temperature condition (a: 190 °C; b: 210°C; c: 200 °C), and "#" indicates the aging time (from 1 to 10). Three small square specimens were prepared for some initial control experiments with the FTIR characterization (labelled (A-H)-0, (A-H)-s-1, and (A-H)-s-2). Figure S1 shows an example of the distribution of the specimens in a film. In addition, in order to minimize the effect of any eventual inhomogeneity within the PEI films, the specimens corresponding to each condition had a different location within the film for each of the eight films.

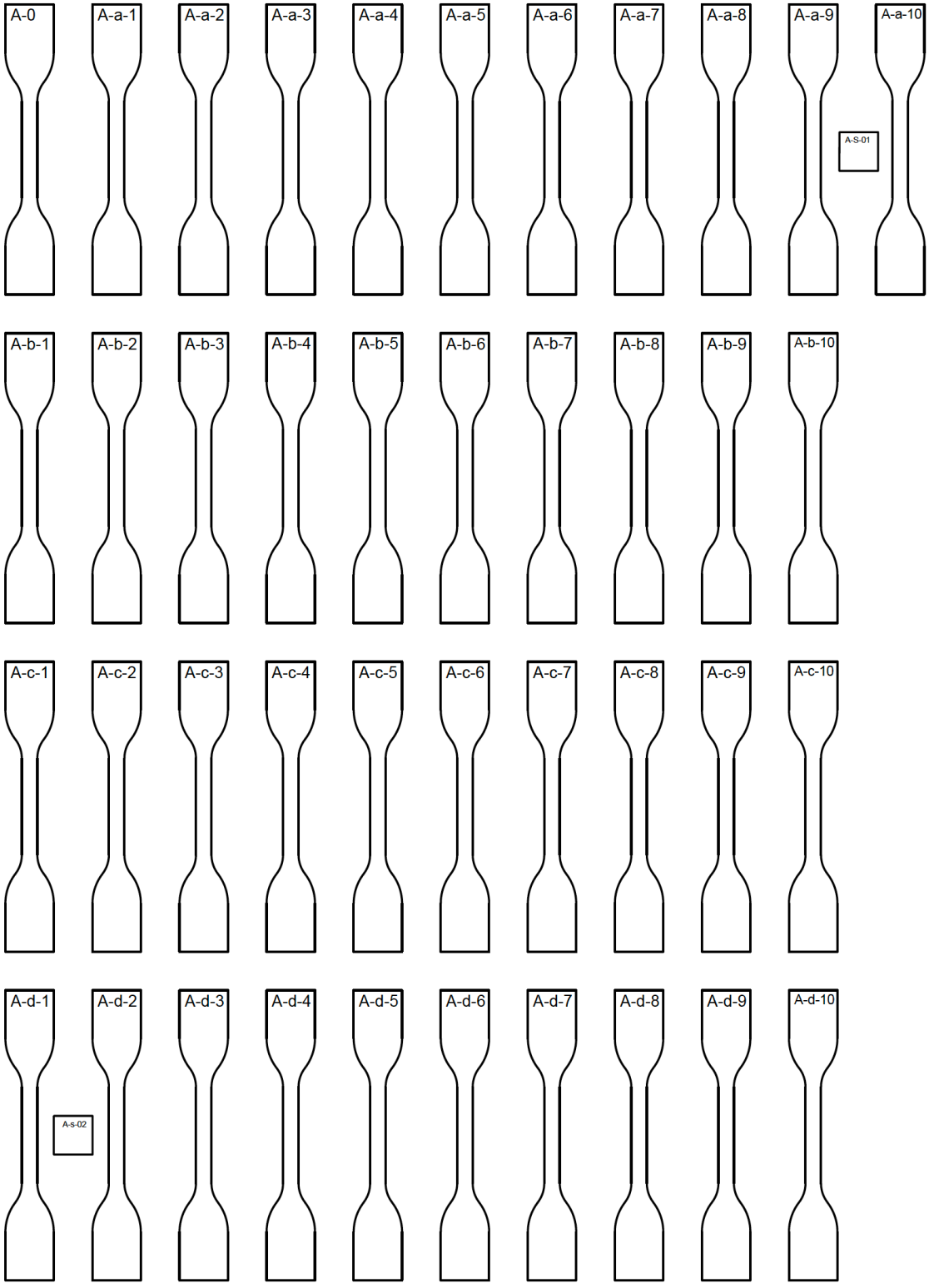

Figure S1: Distribution of the specimens on film A

S2. Accelerated thermal aging program

The convection oven has two shelves (Figure S2); each shelf can hold 40 suspended specimens. The temperature distribution in the oven was assessed using eight thermocouples distributed throughout the oven (Figure S3). The measurement was done at the following temperatures: 50 °C, 100 °C, 150 °C, 200 °C, 250 °C and 300 °C. The temperatures measured are listed in Table S1.

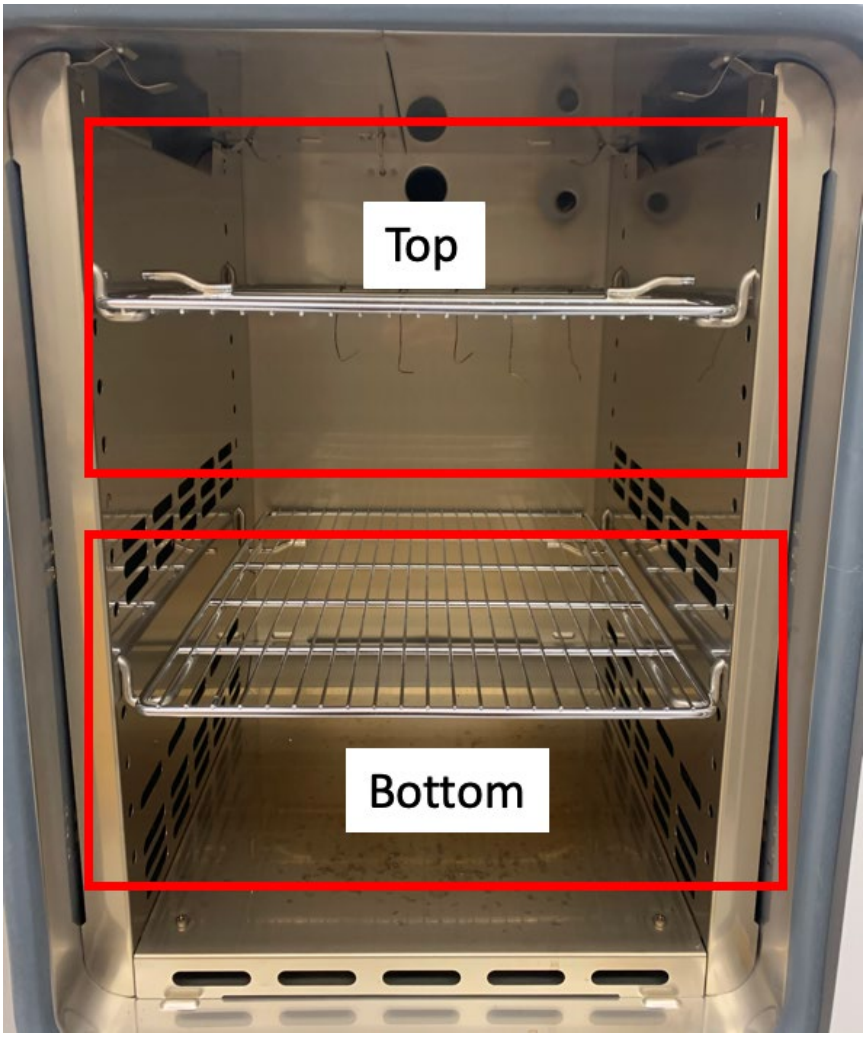

Figure S2: Convection oven used for the thermal aging of the PEI specimens

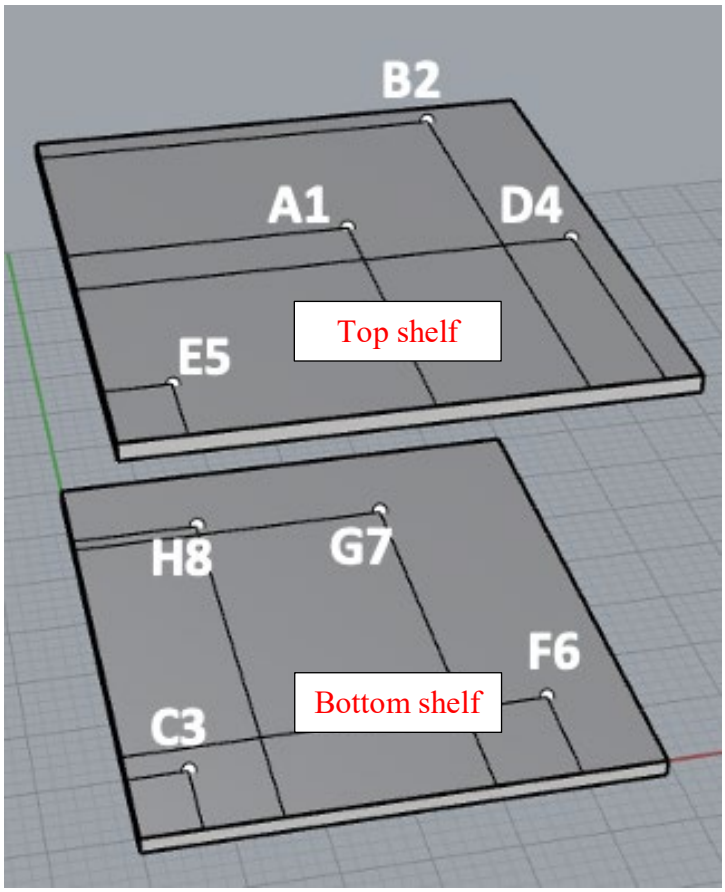

Figure S3: Distribution of the eight thermocouples on top and bottom shelf of the oven

An single factor ANOVA analysis was performed on the temperature data of the eight thermocouples at each oven set temperature (50 °C, 100 °C, 150 °C, 200 °C, 250 °C, and 300 °C). It showed that there is no significant difference in temperature between the different locations in the oven ($p = 0.99$, Total sample size $N = 48$). Table S1 also provides the average value of the temperatures recorded by the eight thermocouples. As there is a difference between the average temperature by the thermocouples and the set value in the oven, a correction was made to compensate for the difference between the oven set temperature and the temperature experienced by the specimens in the oven.

Table S1 Temperature data from the eight thermocouples in the oven

Oven set temperature (°C)	50	100	150	200	250	300
Thermocouple 1	51.9	97.9	144.8	191.2	240.3	288.6
Thermocouple 2	50.9	91.3	142.8	188.9	239.6	286.7
Thermocouple 3	50.5	97.1	144.0	188.9	238.3	287.3
Thermocouple 4	51.9	96.2	141.8	186.4	232.8	265.3
Thermocouple 5	50.6	97.8	146.7	191.5	238.3	287.7
Thermocouple 6	50.3	97.0	143.1	188.6	233.8	280.2
Thermocouple 7	50.7	96.9	143.4	191.2	240.9	291.6
Thermocouple 8	51.6	98.5	146.1	193.4	243.0	293.0
Average temperature measured by the thermocouples (°C)	51.1 ± 0.6	96.5 ± 0.7	144 ±2	190 ±2	238 ±3	285±8

In addition, the temperature was recorded for 15 min after the door of the oven was opened and closed to simulate the operation associated with specimen collection (Figure S4). A temperature drop was observed when the oven door was opened. But the temperature came back rapidly to the set value after the door was closed. This opening and closing of the door when collecting the specimens is not expected to affect the aging of the specimens in the oven, especially since great care is been taken in minimizing the time the door is left opened during the collection operation.

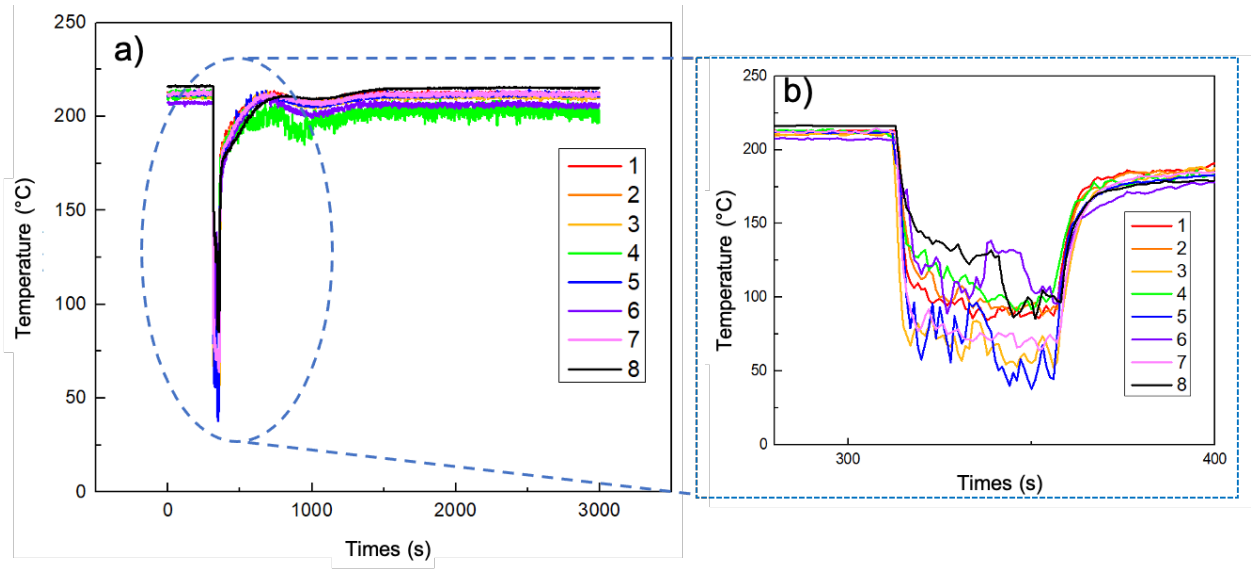

Figure S4: Variation in the temperature over time during the opening and closing of the oven door. The graph in b) provides a close-up view on the opening and closing event. The numbers in the legend correspond to the eight thermocouples.

In order to minimize any effect of the temperature differences inside the oven, the specimens were positioned so that the replicates for each condition are distributed over the oven. This distribution is illustrated in Figure S5 and Table S2. Special attention was also taken to maintain a certain distance between the specimens and with the oven walls. Tables S3 to S5 show the specimen codes for the different temperature and time conditions: the specimens were exposed at 190 °C for up to 12 weeks, at 200 °C for up to 16 weeks, and at 210 °C for up to 8 weeks.

Table S2 Distribution of the specimens in the oven. Samples shown in the grey area correspond to the top shelf while samples shown in the white area correspond to the bottom shelf of the oven.

Sample # / Film #	(a-d)-1	(a-d)-2	(a-d)-3	(a-d)-4	(a-d)-5	(a-d)-6	(a-d)-7	(a-d)-8	(a-d)-9	(a-d)-10
A	1	2	3	4	5	6	7	8	9	10
B	13	16	12	20	17	14	11	15	18	19
C	22	27	26	23	30	28	29	24	25	21
D	36	33	37	31	32	40	34	39	38	35
E	48	45	43	44	49	42	47	41	50	46
F	54	58	55	59	51	57	52	53	56	60
G	69	61	70	65	68	64	66	67	63	62
H	80	79	78	77	76	75	74	73	72	71

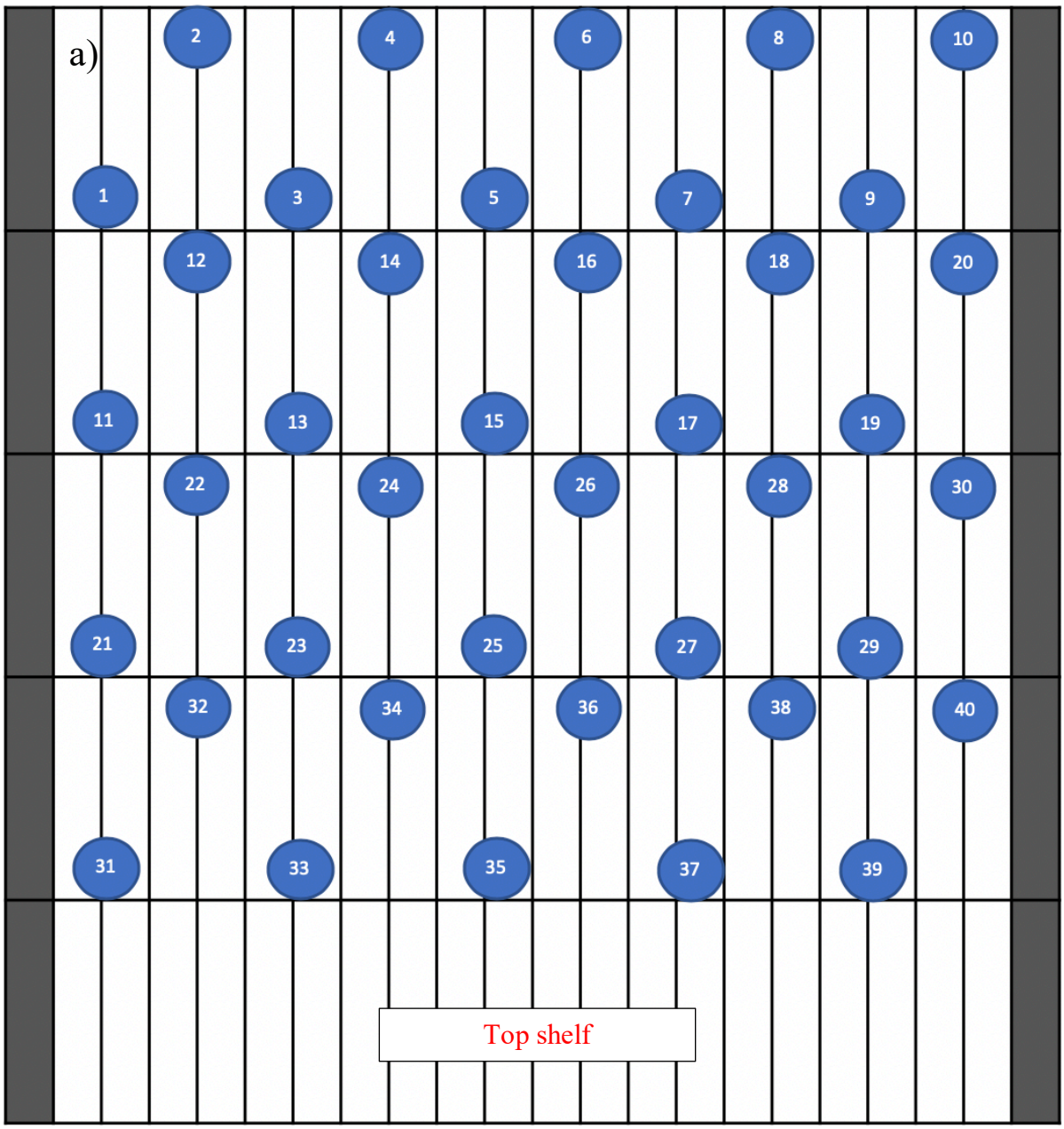
a)
1
2
3
4
5
6
7
8
9
10
11
12
13
14
15
16
17
18
19
20
21
22
23
24
25
26
27
28
29
30
31
32
33
34
35
36
37
38
39
40
Top shelf

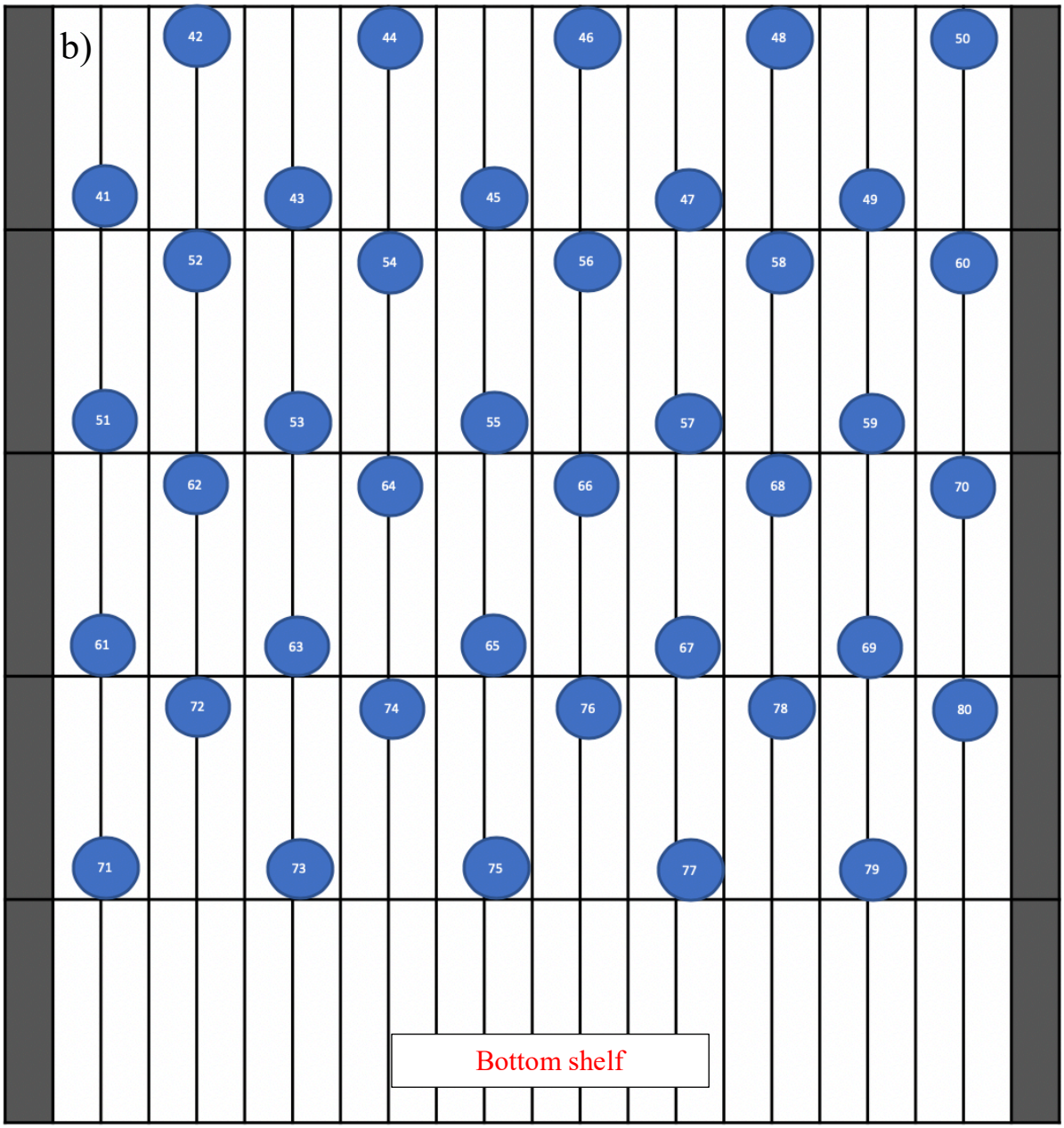

Figure S5: Specimen distribution a) on the top and b) bottom shelves of the oven

Table S3: Identification of the specimens subjected to thermal aging at 190 °C.

Aging time (week) / Specimen	1	2	3	4	5	6	8	10	12
(A-H)-a-1									
(A-H)-a-2									
(A-H)-a-3									
(A-H)-a-4									
(A-H)-a-5									
(A-H)-a-6									
(A-H)-a-7									
(A-H)-a-8									

Table S4: Identification of the specimens subjected to thermal aging at 200 °C.

Aging time (week) / Specimen	2	4	6	8	10	12	13	14	15	16
(A-H)-b-1										
(A-H)-b-2										
(A-H)-b-3										
(A-H)-b-4										
(A-H)-b-5										
(A-H)-b-6										
(A-H)-b-7										
(A-H)-b-8										
(A-H)-b-9										
(A-H)-b-10										

Table S5: Identification of the specimens subjected to thermal aging at 210 ℃.

Aging time(week) / Specimen	1	2	3	4	5	6	7	8
(A-H)-c-1								
(A-H)-c-2								
(A-H)-c-3								
(A-H)-c-4								
(A-H)-c-5								
(A-H)-c-6								
(A-H)-c-7								
(A-H)-c-8								

S3. Crack surface area calculation

Figure S6 provides an example of FE-SEM image of the cracks. It also shows the "color histogram" feature applied to the imported FE-SEM image of the cracks that colors the cracks in black whereas the rest of the sample surface appears red.

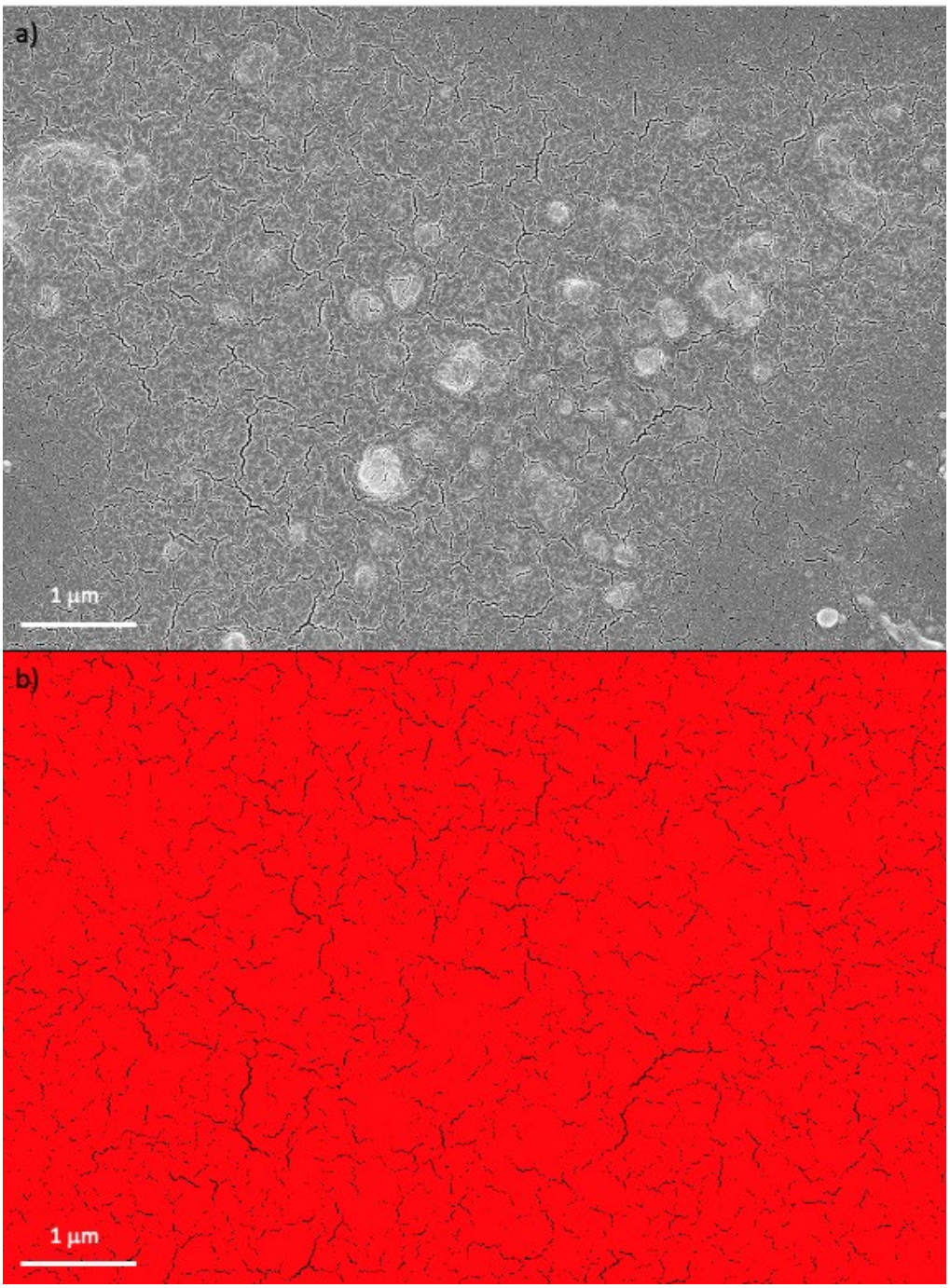

Figure S6: a) FE-SEM image showing the cracks (8 weeks of aging at 210 °C); b) "color histogram" feature applied to the imported FE-SEM image of the cracks, in which the cracks are colored in black and the rest of the sample surface is colored in red.

S4. Differential scanning calorimetry (DSC) curve fitting

Figure S7 and S8 illustrate the analysis of the DSC profiles.

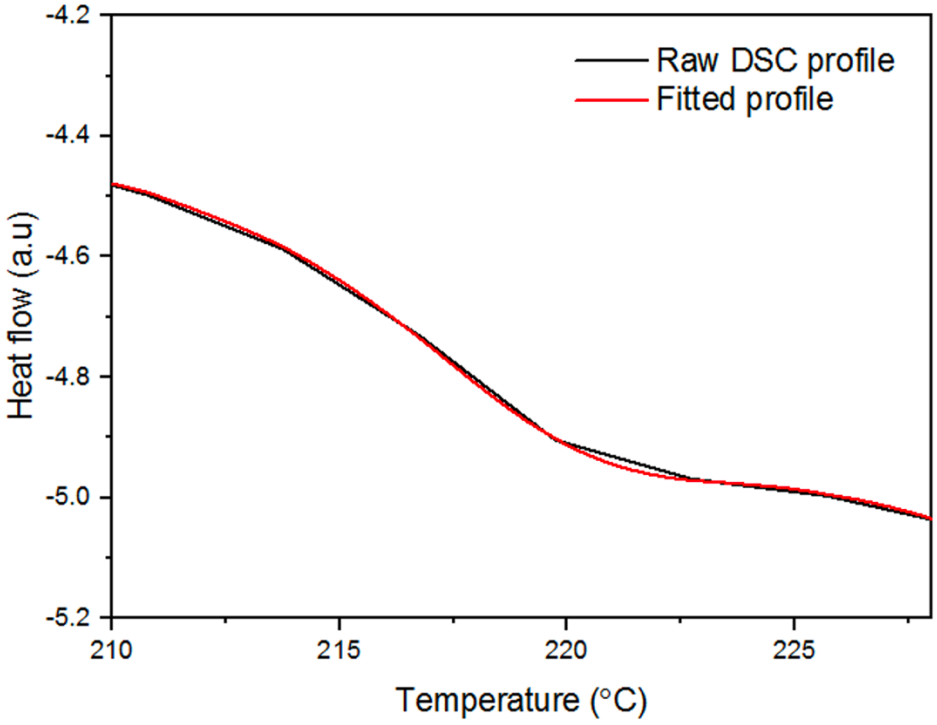

Figure S7: Bi-Gaussian fitting of the differential scanning calorimetry curve

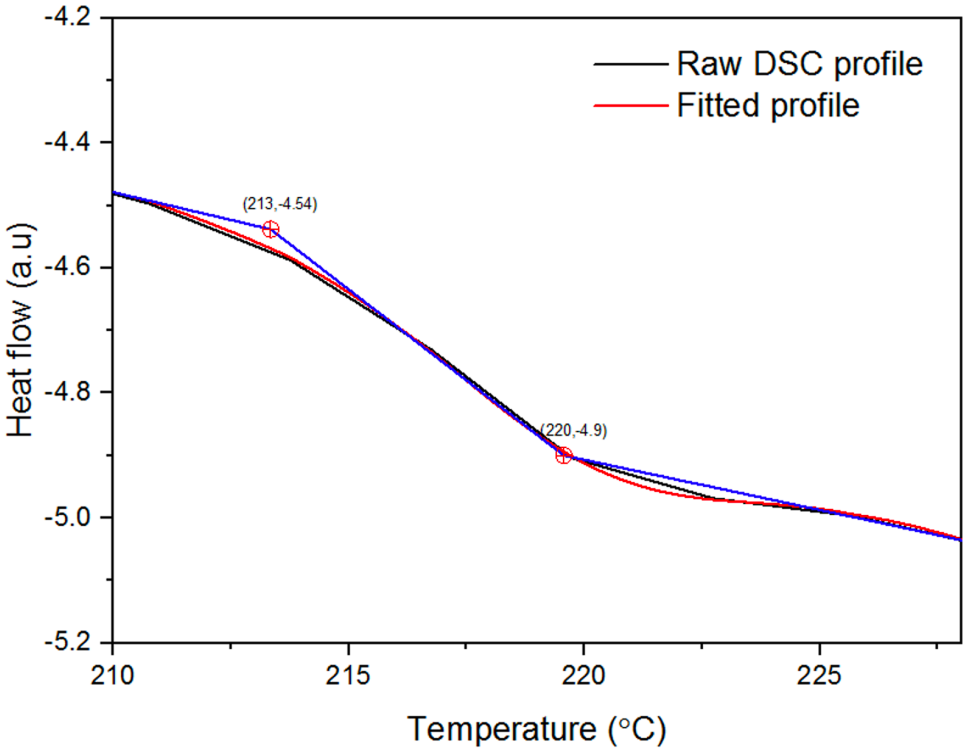

Figure S8: Determination of the onset and end point temperatures from the tangential lines on the fitted differential scanning calorimetry curve.

S5. Statistical analysis (one-way ANOVA)

After evaluating the statistical significance using a one-way ANOVA, the post-hoc analysis was performed to verify which conditions were statistically different from the others. The Tukey HSD (Honestly Significant Difference) test was used as a post-hoc analysis to indicate if any group is significantly different from other groups. During the Tukey analysis, critical q-values are required; these were obtained from a table of studentized q values.[2] If the HSD value is larger than the critical q-value, the difference of the means is significant at the specific confidence level. The HSD and the mean square within a group MS_w are calculated by Equation S1 and S2.

$$\mathrm{HSD} = \mathrm{q}\sqrt{\frac{\mathrm{MS_w}}{\mathrm{n}}} \quad \text{(S1)}$$

$$MS_w = \frac{sum\ of\ squares\ within\ group}{n-1} \quad \text{(S2)}$$

where q is the critical q-value from studentized range table and n is the number of specimens in each group.

S6. ANOVA analysis for the change in the glass transition temperature

From a single-factor ANOVA analysis, a p-value of 1.7×10^{-7} was obtained (n=20). The 95% confidence interval is 217 to 220. The post-hoc analysis by Tukey's HSD test showed that the change in the glass transition temperature was statistically significant during the thermal aging (Table S6).

Table S6: Post-hoc analysis for the change in glass transition temperature during thermal aging. The critical q value is 4.046.

Comparing condition	Mean difference	HSD value	Significance
4 weeks vs. 0 week	5.73	1.83	Yes
6 weeks vs. 0 week	1.90		Yes
4 weeks vs. 6 weeks	3.83		Yes
8 weeks vs. 0 week	0.39		No
8 weeks vs. 4 weeks	6.12		Yes
8 weeks vs. 6 weeks	2.29		Yes

S7. ANOVA analysis of various TGA weight loss characteristic temperatures

Table S7 shows the p-value of various weight loss characteristic temperatures and 95 % confidence intervals of each temperature. We observe that $T_{5\%}$ and $T_{initial}$ shows some statistically significant changes during the thermal aging. The post-hoc analysis of $T_{5\%}$ and $T_{initial}$ reveals that the only statistically significant difference is between 0 week (control) and 8 weeks (Table S8 and S9). On the other hand, the changes in $T_{2nd\ max\ rate}$ were not statistically different and $T_{1st\ max\ rate}$ experienced no change during thermal aging.

Table S7 The p-value of various weight loss temperatures and 95 % confidence intervals

Parameter / **Condition**	**$T_{5\%}$ (°C)**	**$T_{initial}$ (°C)**	**$T_{1st\ max\ rate}$ (°C)**	**$T_{2nd\ max\ rate}$ (°C)**
p-value	0.02	0.01	0.24	0.4
95 % confidence interval	452 - 472	542 - 546	561 - 564	668 - 688

Table S8: Post-hoc analysis for changes in $T_{initial}$ during thermal aging. The critical q value is 4.529.

Compared conditions	Mean difference	HSD value	Significance
4 weeks vs. 0 week	19.62	29.27	No
6 weeks vs. 0 week	13.72		No
6 weeks vs. 4 weeks	5.90		No
8 weeks vs. 0 week	37.84		Yes
8 weeks vs. 4 weeks	18.22		No
8 weeks vs. 6 weeks	24.12		No

Table S9: Post-hoc analysis for changes in $T_{5\%}$ during thermal aging. The critical q value is 4.529.

Compared conditions	Mean difference	HSD value	Significance
4 weeks vs. 0 week	2.34	29.26531	No
6 weeks vs. 0 week	3.66		No

6 weeks vs. 4 weeks	1.32		No
8 weeks vs. 0 week	7.47		Yes
8 weeks vs. 4 weeks	5.13		No
8 weeks vs. 6 weeks	3.81		No

S8. ANOVA analysis of the FTIR peak area changes

The one-way ANOVA analysis of the change in the 1215 cm^{-1} peak area gave a p-value of 8.6×10^{-10} (n=40); the 95% confidence interval is 6.88 to 7.06. A post-hoc analysis was conducted to see which group is different from other groups (table S10). The peak area of the control and 2 weeks aged PEI was statistically different from the results at all other aging conditions. In addition, 6 and 8 weeks of aging also showed statistically significant differences.

Table S10*:* Post-hoc analysis for peak area changes at 1215 cm^{-1}. The critical q value is 4.066.

Compared conditions	Mean difference	HSD value	Significance
2 weeks vs. 0 week	0.07	0.38	No
4 weeks vs. 0 week	0.61		Yes
4 weeks vs. 2 weeks	0.68		Yes
6 weeks vs. 0 week	0.84		Yes
6 weeks vs. 2 weeks	0.91		Yes
6 weeks vs. 4 weeks	0.23		No
8 weeks vs. 0 week	0.41		Yes
8 weeks vs. 2 weeks	0.49		Yes
8 weeks vs. 4 weeks	0.20		No
8 weeks vs. 6 weeks	0.43		Yes

The ANOVA gave a p-value of 5.3×10^{-6} (n=40) for the peak area of isopropylidene group; the 95% confidence interval is 1.23 to 1.27. The peak area of the control and 2 weeks aged PEI was statistically different from the results at 6 and 8 weeks aged PEI. Among the other pairs of conditions, only the difference between the peak areas at 4 and 8 weeks of aging was statistically significant (Table S11).

Table S11: Post-hoc analysis for peak area changing of 1172 cm^{-1}. The critical q value is 4.066.

Comparing conditions	Mean difference	HSD value	Significance
2 weeks vs. 0 week	0.02	0.03	No
4 weeks vs. 0 week	0.03		No
4 weeks vs. 2 weeks	0.01		No
6 weeks vs. 0 week	0.05		Yes
6 weeks vs. 2 weeks	0.03		Yes
6 weeks vs. 4 weeks	0.02		No
8 weeks vs. 0 week	0.06		Yes
8 weeks vs. 2 weeks	0.04		Yes
8 weeks vs. 4 weeks	0.03		Yes
8 weeks vs. 6 weeks	0.01		No

S9. Example of stress-strain curve for the aged PEI specimens

Figure S9 shows an example of stress-strain curve for the aged PEI specimens.

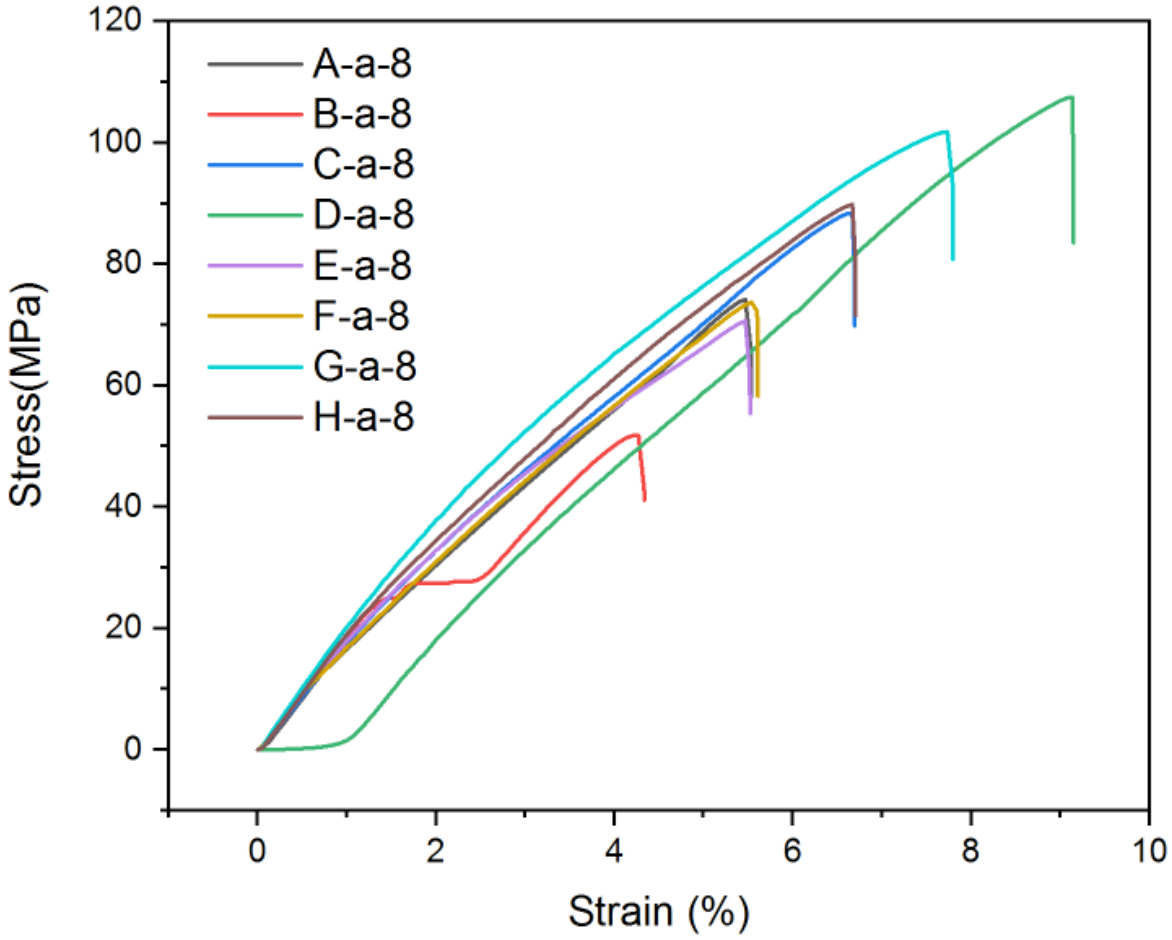

Figure S9: Stress-strain curve for the eight PEI specimens after 8 weeks of aging of 210 °C

S10. Fourier Transform Infrared (FTIR) peak treatment

Once the peaks of interest were identified, they were deconvoluted so that their individual area is calculated. Figure S10 illustrates the process of peak deconvolution and Figure S11 shows the peak area calculation process. The raw FTIR spectra were deconvoluted and analyzed using the Peak Analyzer function in Origin (Version 2020b). First, we performed a baseline correction of the FTIR spectrum by interpolation between linear sections at both extremities of the peak series. The software then performed the deconvolution of the FTIR spectrum into several Gaussian peaks. The areas of these peaks were calculated using the peak integration function in the software. To allow a comparison between different FTIR spectra, the peak area is divided by the area of a reference peak.[1] For PEI, the reference peak corresponds to the aromatic ring stretching at 838 cm^{-1}. In order to keep the reference peak area constant between the different spectra measured, the spectra were normalized such that the reference peak area was scaled to unity.

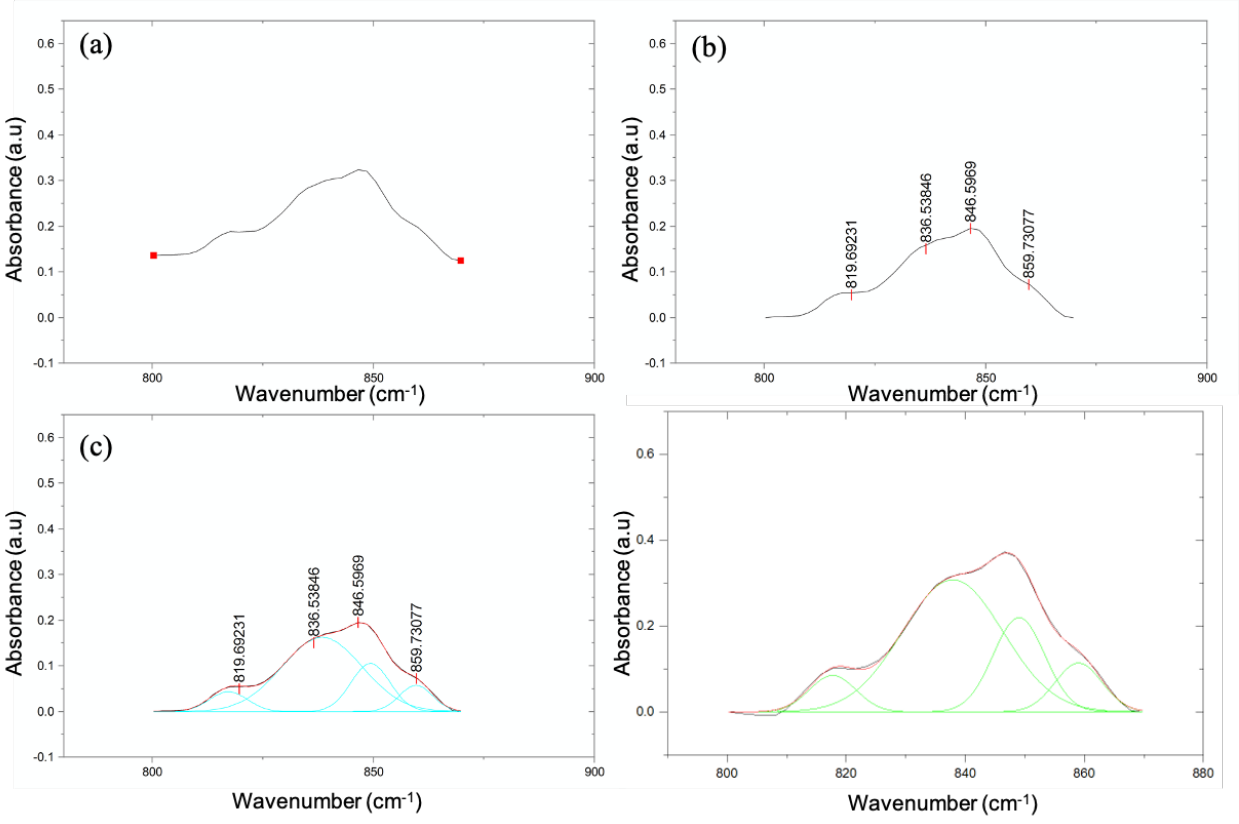

Figure S10 Process of deconvolution of the FTIR spectroscopy spectra: (a) selection of two points that encompass the overlapping peaks; (b) peak identification; (c) fitting of the Gaussian peaks; (d) deconvoluted peaks.

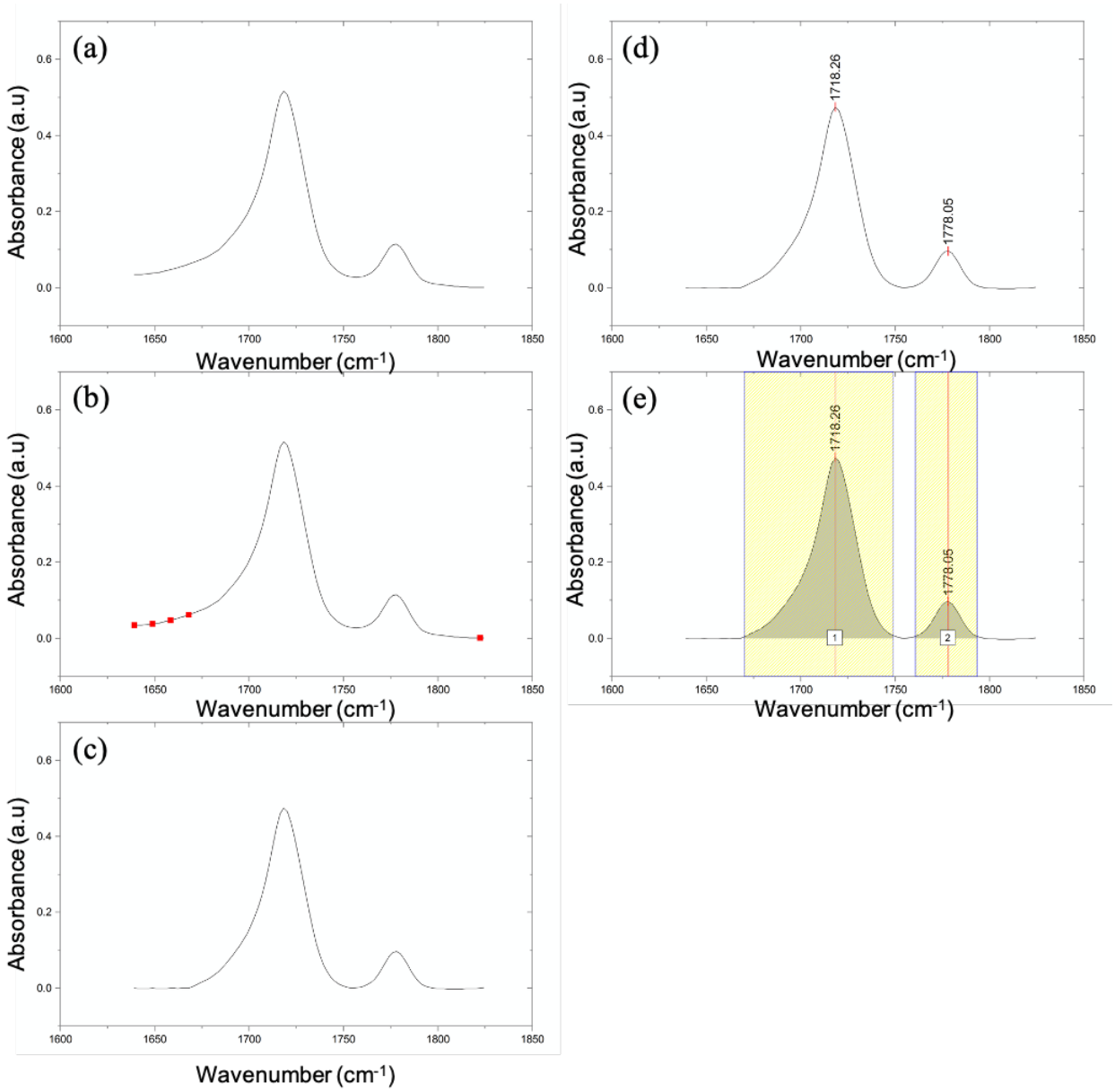

Figure S11 Calculation of the FTIR spectroscopy peak area: (a) selection of the wavenumber range; (b)-(c) baseline correction; (d) peak identification; (e) peak area integration.

For each aging time, spectra were collected for the eight replicates. Depending on the temperature, 8 or 10 aging times were used. When one adds the control condition, this leads to 72 or 88 spectra being compared (see the example in Figure S12 a) for the 210 °C case). To facilitate the comparison of the results at the different conditions, the eight spectra corresponding to the eight replicates measured for each condition were merged into one spectrum using the SpectraGryph software (http://spectragryph.com, Oberstdorf, Germany). The merging process

involves extrapolating between the gaps of the spectra and averaging the overlaps in the spectra. This process is shown in Figure S12 in the case of the spectra for the specimens aged at 210 °C for the entire wavelength range (Figure S12 a and b) and for the 1172 cm^{-1} peak (Figure S12 c and d).

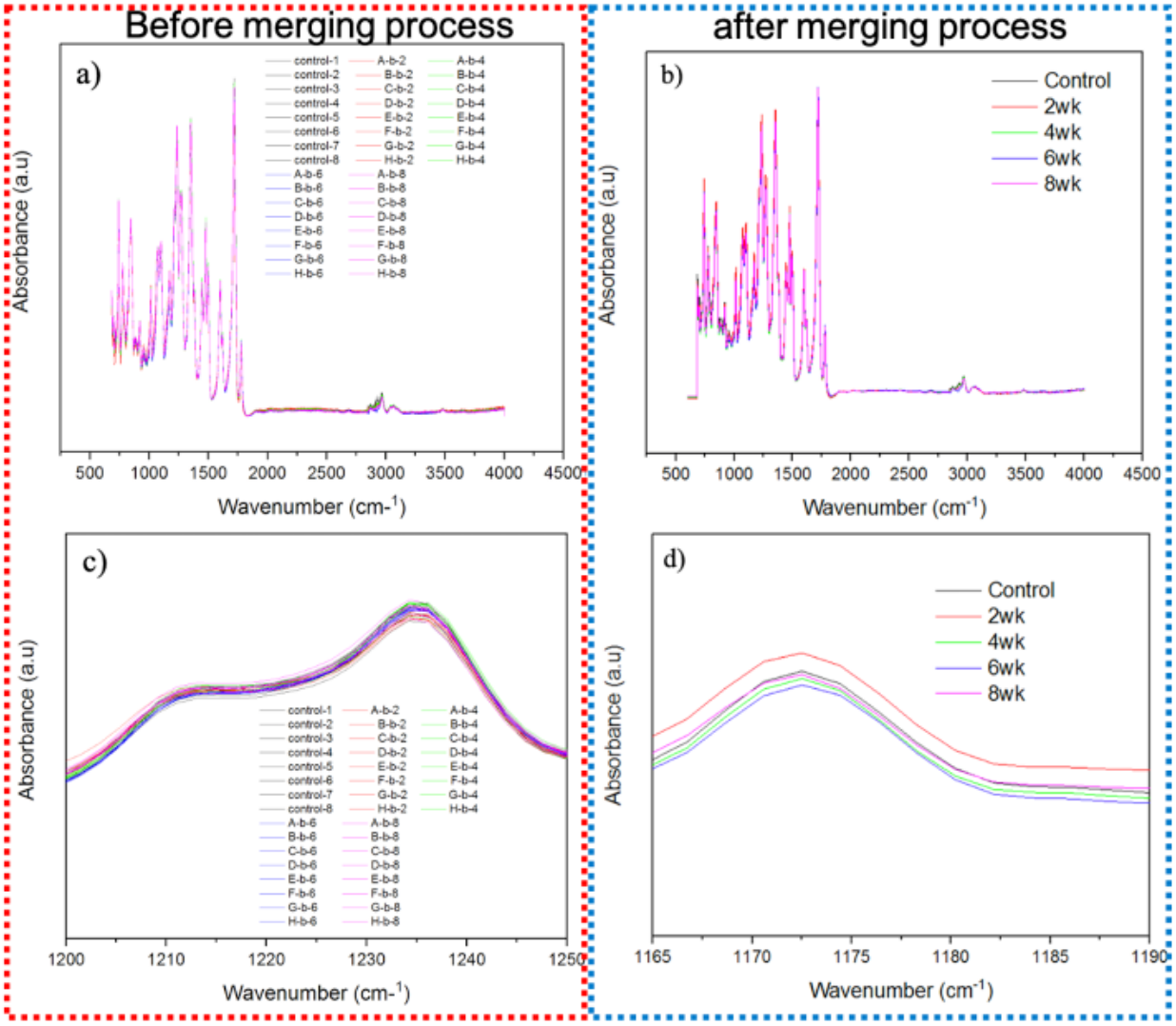

Figure S12: FTIR spectroscopy spectra for the unaged condition and for the specimens aged at 210 °C for 2, 4, 6 and 8 weeks: a) all 40 spectra over the entire wavelength range; b) after merging the spectra of the 8 replicates; c) at 1172 cm^{-1} peak for the 40 spectra; and d) after the merging process (5 spectra).

References

[1] Amancio-Filho, S. T.; Roeder, J.; Nunes, S. P.; dos Santos, J. F.; Beckmann, F. Thermal Degradation of Polyetherimide Joined by Friction Riveting (FricRiveting). Part I: Influence of Rotation Speed. *Polym. Degrad. Stab.* **2008**, *93* (8), 1529–1538. https://doi.org/https://doi.org/10.1016/j.polymdegradstab.2008.05.019.

[2] Studentized range q table https://www.stat.purdue.edu/~lingsong/teaching/2018fall/q-table.pdf.